ISSN (print): 1698-6180. ISSN (online): 1886-7995
www.ucm.es/info/estratig/journal.htm

Journal of Iberian Geology 35 (2) 2009: 85-125

Journal of Iberian Geology
AN INTERNATIONAL PUBLICATION OF EARTH SCIENCES

The basal tectonic mélange of the Cabo Ortegal Complex (NW Iberian Massif): a key unit in the suture of Pangea

La mélange tectónica basal del Complejo de Cabo Ortegal (NW del Macizo Ibérico): una unidad clave en la sutura de Pangea

R. Arenas*[1], S. Sánchez Martínez[1], P. Castiñeiras[1], T.E. Jeffries[2], R. Díez Fernández[3], P.Andonaegui[1]

[1]Departamento de Petrología y Geoquímica and Instituto de Geología Económica (CSIC-UCM) Facultad de Ciencias Geológicas, Universidad Complutense de Madrid, 28040 Madrid, Spain.
**corresponding author: arenas@geo.ucm.es*
[2]Department of Mineralogy. The Natural History Museum. Cromwell Road. London SW7 5BD UK.
[3]Departamento de Geología. Universidad de Salamanca. 37008 Salamanca, Spain

Received: 26/01/09 / Accepted: 27/05/09

Abstract

Recent field work and mapping in the lower units of the Cabo Ortegal Complex provided new data about the tectonic mélange that appears in the lowest structural position: the Somozas Mélange. This mélange unit with average thickness of 1800 m is restricted to the eastern part of the complex, and is located at the advancing front of the allochthonous complexes of NW Iberia. Three rock units are involved in the mélange: 1) an ophiolitic mélange consisting of igneous rocks mixed with serpentinites; 2) a metasedimentary unit with phyllites and phyllonites, with scarce conglomerates, marbles and quartzites; 3) high-T metamorphic rocks with varied types of amphibolites and orthogneisses.

Two granitic rocks within the ophiolitic mélange were dated using U-Pb zircon geochronology at 527 ± 2 Ma and 499 ± 1 Ma. Two different series of igneous rocks can be distinguished in this mélange. The first series consists of gabbros, diorites, granitoids and basalts-basaltic andesites with calc-alkaline affinities. The second series contains common basaltic rocks, diabasic dikes and gabbros with chemical compositions typical of island-arc tholeiites. Both igneous series shared a common geographic setting, but the island-arc tholeiites are younger than the calc-alkaline igneous rocks. The two igneous series were probably generated in a mature volcanic arc located along the periphery of Gondwana. In the metasedimentary unit, a conglomerate from a large tectonic block included in serpentinites yielded age populations of detrital zircons suggesting that the sediments were deposited along the periphery of the West-African Craton. This conglomerate contains a large number of zircons (n = 24) with ages ranging 630-464 Ma, probably representing the chronology of the Pan-African event, including the magmatic activity in the volcanic arc where the igneous lithologies involved in the mélange were generated. The maximum age of sedimentation for this conglomerate is estimated as latest Cambrian – earliest Ordovician, and constraints the end of the magmatic activity in the volcanic-arc. Within the unit of high-T rocks,

an orthogneiss yields a U-Pb protolith age of 485 ± 6 Ma, which is similar to other ages of igneous rocks in the basal allochthonous terrane in NW Iberia. The three rock assemblages forming part of the Somozas Mélange may be linked to the evolution of a mature peri-Gondwanan volcanic arc. This volcanic arc was affected by pronounced extension which caused the opening of intra-arc basins, culminating the rifting and subsequent drift of the external parts of the arc during the opening of the Rheic Ocean. This opening started during a time interval constrained by the peak activity in a mature volcanic arc (c. 527-499 Ma) and the generation of intra-arc basins around the Cambrian-Ordovician boundary.

Tectonic mélanges including high-P rocks have been classically related to subduction zone environments. Regional relationships in NW Iberia and the nature of the rock units involved in the Somozas Mélange, suggest that two different subduction zones generated during oblique convergence and collision between Gondwana and Laurussia were active during the final stages of the assembly of Pangea. The first related to the underthrusting beneath Laurussia of the most external Gondwana margin (c. 370 Ma). The second subduction zone was a new one which accreted later remnants of a peri-Gondwanan arc and sediments of the continental margin below a layer of exhumed high pressure rocks. This oblique collision finished the closure of the Rheic Ocean and contributes to define the new oceanic domain located to the East of Pangea, the Palaeotethys.

Keywords: Ophiolitic mélange, Rheic Ocean, island arc, suture of Pangea, U-Pb zircon geochronology, Variscan Belt, Cabo Ortegal Complex.

Resumen

Nuevos datos de campo y cartográficos en las unidades inferiores del Complejo de Cabo Ortegal, han proporcionado información relevante sobre la mélange tectónica situada en la posición estructural inferior: la Mélange de Somozas. Esta unidad de mélange tiene una potencia media de unos 1800 m y su aparición está restringida a la parte oriental del complejo; representa por tanto una gran unidad de mezcla localizada en el frente de avance de los complejos alóctonos del NW de Iberia. Tres conjuntos litológicos diferentes se distinguen en la mélange: 1) un conjunto formado por rocas ígneas mezcladas con serpentinitas, formando una mélange ofiolítica típica; 2) un conjunto metasedimentario con filitas y filonitas, con escasos conglomerados, mármoles y cuarcitas; 3) rocas metamórficas de alta-T con tipos variados de anfibolitas y ortogneises.

Dos rocas graníticas incluidas en la mélange ofiolítica han sido datadas mediante geocronología U-Pb en 527 ± 2 Ma y 499 ± 1 Ma. La mélange ofiolítica contiene dos series diferentes de rocas ígneas. Una primera serie está formada por gabros, dioritas, granitoides y basaltos-andesitas basálticas con afinidades calcoalcalinas. La segunda serie contiene diques diabásicos, gabros y rocas basálticas comunes con composiciones químicas típicas de toleitas de arco-isla. Ambas series compartieron un marco geográfico común, pero las toleitas de arco-isla son más jóvenes que las rocas ígneas calcoalcalinas, y fueron generadas en un arco volcánico maduro situado en la periferia de Gondwana. Dentro del conjunto de rocas metasedimentarias, un conglomerado procedente de un gran bloque tectónico incluido en serpentinitas ha proporcionado poblaciones de edades de circones detríticos que indican que su sedimentación se produjo en la periferia del Cratón del Oeste de África. Este conglomerado contiene una población principal de circones (24 cristales) con edades que oscilan entre 630-464 Ma, que reflejan la cronología del evento Pan-Africano y también la actividad magmática en el arco volcánico donde se generaron las dos series ígneas existentes en la mélange ofiolítica. La edad máxima de sedimentación de este conglomerado se sitúa en el límite Cámbrico-Ordovícico, y puede considerarse también una edad de referencia para la terminación de la actividad magmática principal en el arco volcánico. Dentro del conjunto de rocas de alta-T, un ortogneis ha proporcionado una edad U-Pb del protolito de 485 ± 6 Ma. Esta edad es similar a otras edades de rocas ígneas pertenecientes al terreno alóctono basal del NW de Iberia. Los tres conjuntos de rocas que forman parte de la Mélange de Somozas pueden relacionarse con la evolución de un arco volcánico peri-Gondwánico maduro. Este arco volcánico acabó siendo afectado por una extensión pronunciada que favoreció la apertura de cuencas de intra-arco, y finalmente la separación y posterior deriva de las partes externas del arco durante la apertura del Océano Rheico. En concreto, el comienzo de la apertura se produjo en algún momento situado entre el episodio de actividad magmática principal en el arco volcánico maduro (c. 527-499 Ma), y la generación de cuencas de intra-arco hacia el límite Cámbrico-Ordovícico.

Las mélanges tectónicas que incluyen rocas de alta-P se han relacionado clásicamente con contextos de subducción. Las relaciones regionales en el NW de Iberia y la naturaleza de las litologías que aparecen en la Mélange de Somozas, sugieren que dos zonas de subducción diferentes, generadas durante la convergencia y colisión oblicuas entre Gondwana y Laurussia, fueron activas durante los estadios finales del ensamblado de Pangea. La primera relacionada con el enterramiento bajo Laurussia del margen más externo de Gondwana (c. 370 Ma). La segunda zona de subducción fue diferente y responsable de la acreción poco después de los restos de un arco peri-Gondwánico y sedimentos del margen continental, bajo una lámina de rocas de alta presión exhumadas. Esta colisión oblicua culminó el cierre del Océano Rheico, contribuyendo a definir el nuevo dominio oceánico situado al Este de Pangea, el Paleotethys.

Palabras clave: Mélange ofiolítica, Océano Rheico, arco de islas, sutura de Pangea, geocronología U-Pb en circones, Cadena Varisca, Complejo de Cabo Ortegal.

1. Introduction

The development of thick tectonic mélanges is documented in several orogenic belts, but in general they are rather unusual units associated to first order tectonic contacts. These common mélanges may have igneous and sedimentary components, but in normal cases all the lithologies involved in the mixing unit can be identified in other terranes represented in the same region. In other words, the most typical mélanges show a tectonic origin but do not include exotic elements. Although they can provide important information about the tectonic history of a given part of a belt, they supply only limited information about the origin of the terranes involved. Conversely, large ophiolitic mélanges are less common and they can reach kilometre-scale thickness and extended continuity. They are characterized by the presence of a serpentinite matrix which surrounds tectonic blocks or slices of very varied lithologies. These ophiolitic mélanges can provide important data about the tectonic setting of the terranes present in the orogenic belt, because they usually include exotic elements that may record tectonothermal histories unknown in the region outside the mélange unit. Several mélanges typically contain high-P rocks that are not represented in the surrounding terranes. In other cases, a given ophiolitic assemblage only exists inside the tectonic mélange and never appears as an independent unit with regional distribution. In these situations, the large ophiolitic mélanges include the only accessible information about terranes with a very exotic nature which are unrecognised outside the mixing unit (MacPherson *et al.*, 2006; Federico *et al.*, 2007). These observations, together with the intensity of the deformation as well as the mantle components, lead to the interpretation of large ophiolitic mélanges as paleo-subduction zones, the most accepted tectonic setting for the generation of large serpentinite mélanges (Gerya *et al.*, 2002; Federico *et al.*, 2007; Osmaston, 2008). In the most typical cases, the tectonic mélange must be generated in the upper part of a subduction zone, because the development of the serpentinitic matrix implies the hydration of the mantle wedge by percolation of ascending fluids from the subducting slab (Gerya *et al.*, 2002). The development of serpentinite mélanges is not possible after the dehydration of the slab, and only mélanges with a peridotite matrix can be considered from a theoretical perspective. These mélanges, if they really exist, are much more uncommon, because the rheology of anhydrous peridotite probably inhibits the development of the tectonic mixing. Different dynamic models have been suggested to explain the precise mechanism involved in the generation of large ophiolitic mélanges (Osmaston, 2008). Recent numerical models have proposed that water loss from the subducting plate produces a low-viscosity serpentinite channel in the overlying mantle wedge, where a forced return flow of subducted material is established (Gerya *et al.*, 2002; Stöckhert and Gerya, 2005; Federico *et al.*, 2007).

Large ophiolitic mélanges can be considered as markers of plate boundaries, and their distribution in orogenic belts is generally restricted to suture zones. However, their development may not been uniform throughout geological time. Many cases of ophiolitic mélanges have been described in circum-Pacific belts (Hirauchi *et al.*, 2008; Kato and Saka, 2003) and in different Cenozoic orogens, such as in the Alps (Federico *et al.*, 2007) or in the Himalayas (Mahéo *et al.*, 2006; Guilmette *et al.*, 2008). However, the references to Paleozoic ophiolitic mélanges are more unusual and the presence of these mixing units in Proterozoic belts is rare (see. Hefferan *et al.*, 2002; Zhang *et al.*, 2008). In the Caledonian Belt of southern Scotland, Kawai *et al.* (2008) have recently described two thick units of ophiolitic mélanges included in the Ballantrae Ophiolite; these mélanges were generated during convergence between Avalonia and Laurentia and the consequent closure of the Iapetus Ocean. In the European Variscan Belt, references to large ophiolitic mélanges are very rare. However, one of these mélanges occurs at the base of the Cabo Ortegal Complex, in the NW of the Iberian Peninsula (Arenas *et al.*, 2007b, 2008), but it has not been described in detail until now. This mélange is involved in the terrane assemblage of the NW Iberian Massif, which is mainly included in the so-called allochthonous complexes of Galicia-Trás-os-Montes. These terranes are considered far-travelled allochthonous units emplaced during the closure of the Rheic Ocean, in the last stages of the Pangea assembly. Therefore, the allochthonous complexes of NW Iberia preserve an excellent section of the Pangea suture. This paper presents a detailed description of the basal ophiolitic mélange of the Cabo Ortegal Complex, the Somozas Mélange, and the geochronology and geochemistry of its most characteristic lithologies. An interpretation of the origin of this important mixing unit, in the context of the convergence and final collision between Gondwana and Laurussia, will be finally discussed.

2. Geological setting

The European Variscan Belt is a Devonian-Carboniferous orogen generated during the progressive collision

between Gondwana and Laurussia following the closure of the Rheic Ocean (Matte, 1991; Martínez Catalán *et al.*, 2007). This orogen can be mapped between the SW of the Iberian Peninsula and the Bohemian Massif, following a curvilinear outline, even though it is affected by some large oroclinal folds. However, the belt probably continues to the east of the Carpathians Arc but its precise location is unknown (Oczlon, 2006). The axial zone of the Variscan Belt is characterized by the presence of several allochthonous complexes comprising exotic terranes with ophiolites and high-P metamorphic rocks (Fig. 1; Arenas *et al.*, 1986). As a whole, these exotic terranes delineate the complex Pangea suture in Europe, which it is rootless and transported inside the allochthonous complexes towards more external regions of the Variscan Belt. In the NW of the Iberian Massif, this suture zone occurs within several allochthonous complexes that are folded into a regional synformal structure. These complexes are remnants of a gigantic pile of nappes, and they contain a representative section of the terranes involved in the most internal part of the suture. In Galicia, NW Spain, the Cabo Ortegal and Órdenes complexes and the

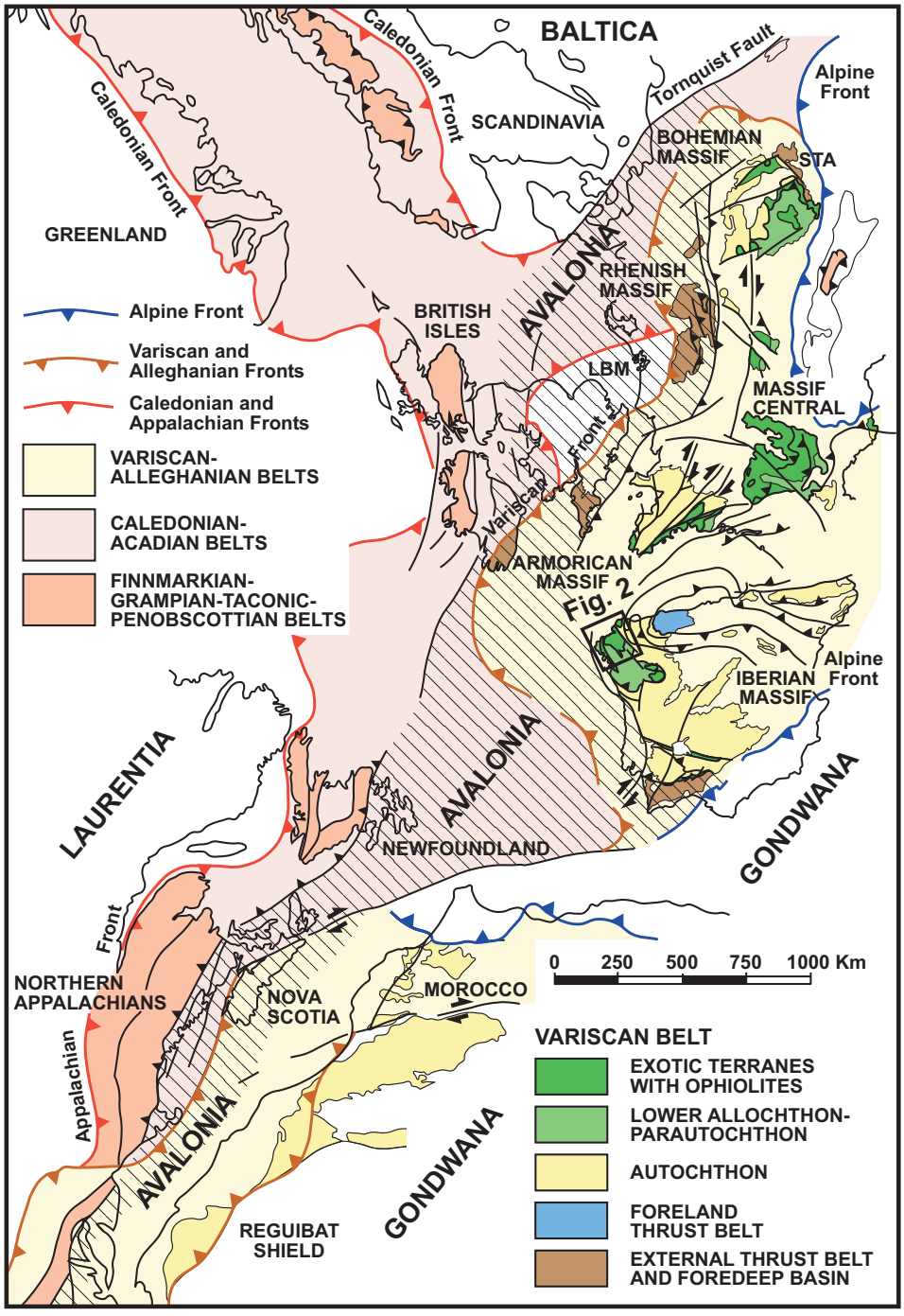

Fig. 1.- Sketch showing the distribution of the Paleozoic orogens in a reconstruction of the Baltica-Laurentia-Gondwana junction developed during the assembly of Pangea. The distribution of the most important domains described in the Variscan Belt are also shown, together with the inferred position of the microcontinent Avalonia and the studied region in NW Iberia. From Martínez Catalán *et al.* (2002). LBM: London-Brabant Massif. STA: Silesian Terrane Assemblage.

Fig. 1.- Esquema con la distribución de los orógenos paleozoicos en una reconstrucción de la unión Báltica-Laurentia-Gondwana generada durante el ensamblado de la Pangea. Se indica la distribución de los dominios más importantes descritos en la Cadena Varisca, junto con la posición deducida del microcontinente Avalonia y la región estudiada en el NW de Iberia. Según Martínez Catalán *et al.* (2002). LBM: Macizo de Londres-Brabant. STA: Asociación de Terrenos de Silesia

Malpica-Tui Unit define a WNW-ESE continuous section across the suture zone (Fig. 2). Considering this section, it is possible to recognize three main exotic terranes included in the allochthonous complexes. These are, from top to bottom, the upper units, the ophiolitic units and the basal units (Fig. 2).

The upper units contain a variety of metasedimentary and igneous rocks, including ultramafic rocks, dated at c. 520-500 Ma, affected by metamorphism ranging between the greenschist and the eclogite facies. Figure 3 shows the most important lithologies involved in the upper units in the Cabo Ortegal Complex; the Órdenes Complex may include an even greater lithological variety (Martínez Catalán *et al.*, 2002). The upper units are an arc-derived terrane with peri-Gondwanan provenance (Fernández-Suarez *et al.*, 2003), characterized by a polymetamorphic tectonothermal evolution. A first intermediate pressure metamorphic event, dated at c. 490-480 Ma (Abati *et al.*, 1999, 2007; Fernández-Suárez *et al.*, 2002), is related to the dynamics of the magmatic arc developed at the Gondwanan margin. Subsequently, the rifting of the arc from the continental margin and its northward drifting is considered coeval with that of the Avalonia microcontinent (Gómez Barreiro *et al.*, 2007; Murphy and Gutiérrez Alonso, 2008). The final accretion of the arc to the southern margin of Laurussia caused a high-P and high-T metamorphic event, identified in the lower part of the upper units of the Cabo Ortegal and Órdenes complexes (Figs. 2 and 3). This high-P event has been dated at c. 390 Ma in the eclogites of the Cabo Ortegal Complex (Ordóñez Casado *et al.*, 2001), and at c. 410-390 Ma in the mafic granulites of the Órdenes and Cabo Ortegal complexes (Fernández-Suárez *et al.*, 2007).

The NW Iberia ophiolitic units, as it is also the case for the rest of ophiolites involved in the Variscan Belt, were generated within the Rheic Ocean domain, and they supply information about the opening and closure of this ocean. Two main ophiolitic assemblages, which are characterized in the field as paired ophiolitic units, can be identified in NW Iberia; the lower ophiolitic units and upper ophiolitic units (Figs. 2 and 3). The lower ophiolitic units consist of a thick pile of greenschists with intercalations of schists and phyllites, and more scarce layers of orthogneisses and ultramafic rocks. The chemical composition of the mafic rocks is characteristic of arc tholeiites, and the protolith age obtained in one of the orthogneisses is c. 500 Ma. These ophiolites were probably generated in a back-arc setting during the first stages of the Rheic Ocean opening (Arenas *et al.*, 2007a). The upper ophiolitic units are consist of metagabbros, metadiabases, amphibolites and ultramafic rocks, dated at c. 395 Ma. The best preserved sections in these ophiolites were described in the Careón Ophiolite (SE of the Órdenes Complex), which exhibit a lithological assemblage representative of a supra-subduction zone ophiolite (Díaz García *et al.*, 1999). This ophiolite neither contains volcanic rocks nor a sheeted dike complex, but it shows frequent doleritic dikes intruding at any level of the gabbroic or ultramafic section, which is considered to be indicative of an extensional context. Sánchez Martínez *et al.* (2007) have proposed that these ophiolites, as other equivalent ophiolites in the Variscan Belt like the Lizard (SW England) or Ślęża (Poland) ophiolites, were generated within an intraoceanic subduction zone which dipped to the north and removed the old and cold N-MORB type lithosphere of the Rheic Ocean. The new oceanic crust generated in this supra-subduction zone context has a composition of arc tholeiites. It represents the last oceanic lithosphere generated inside the Rheic Ocean domain, just slightly before its closure due to the onset of the collision between Gondwana and Laurussia. The accretion time of the Careón-type ophiolites below the high-P upper units is estimated at 380 Ma (Dallmeyer *et al.*, 1997).

The basal units are constituted by schists, paragneises and metagreywackes, and a variety of orthogneisses, frequently very abundant in these units, amphibolites and eclogites. Two igneous series that are different in age can be distinguished in the basal units: a first series with calc-alkaline affinity dated at c. 492 Ma, and a younger series with alkaline-peralkaline composition with protolith ages at c. 472 Ma (see Abati *et al.*, 2009). The basal units show a pervasive high-P and low to intermediate-T metamorphic event and were accreted to the orogenic wedge below the ophiolitic units. Therefore, they are interpreted as a fragment of the most external Gondwanan margin subucted below the orogenic wedge developed in the southern margin of Laurussia (Arenas *et al.*, 1995, 1997; Martínez Catalán *et al.*, 1996). The basal units record the oldest Variscan deformation recognized in the European margin of Gondwana, associated to the final stages of the Pangea assembly. Recent $^{40}Ar/^{39}Ar$ and U-Pb isotopic dating suggests that the subduction of the Gondwanan margin and the coeval high-P metamorphism took place at c. 370 Ma (Rodríguez *et al.* 2003; Abati *et al.*, 2009). The basal units are thrust over a thick allochthonous series of metasedimentary and volcanic rocks, namely the Parautochthon or Lower Allochthon, which has been also described as Schistose Domain. This series is not included in the allochthonous complexes because is similar to the autocthonous sequences of the Central-Iberian Zone, and is not exotic in nature. However, it can be distinguished from the Central Iberian Zone by the

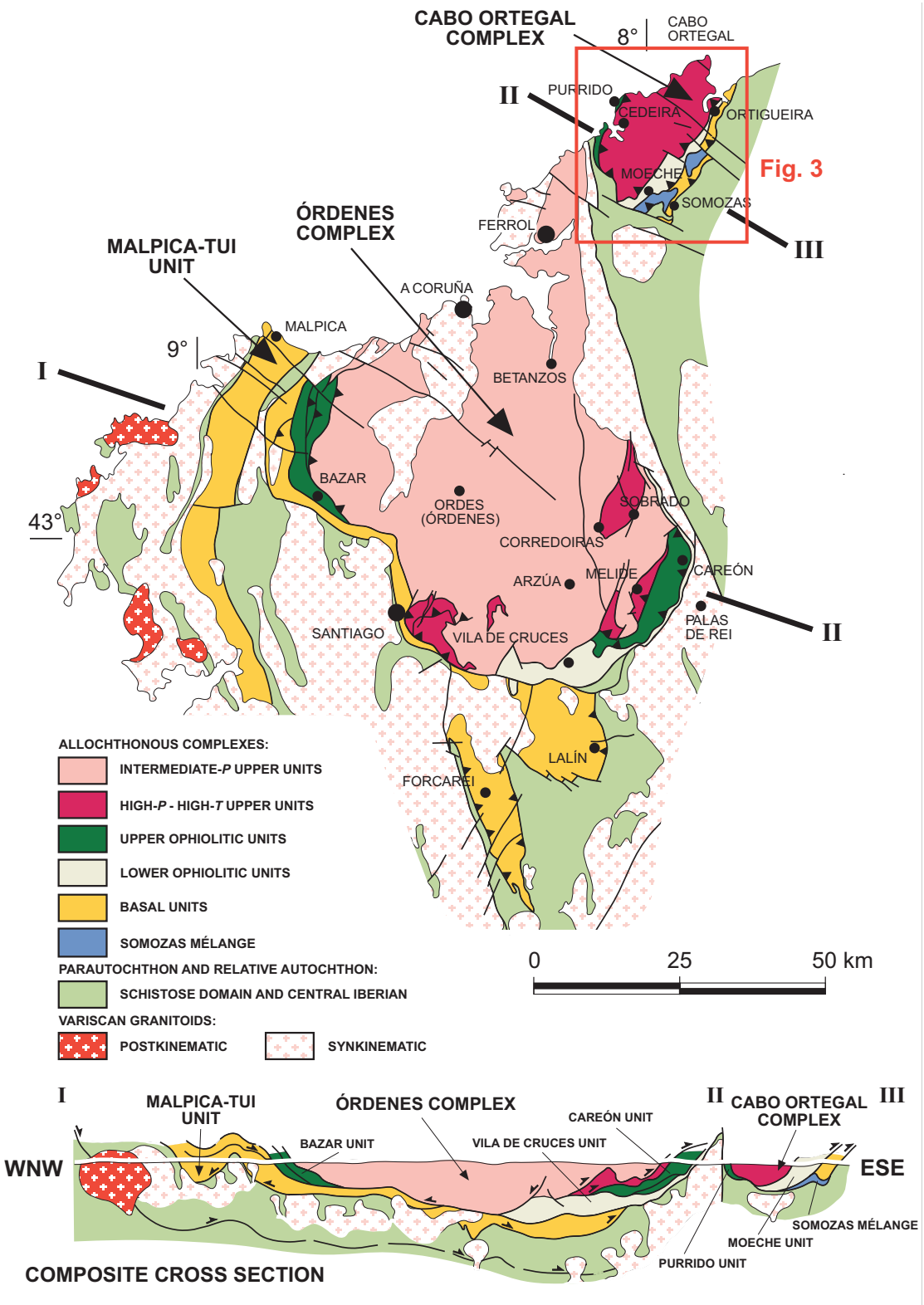

Fig. 2.- Terrane distribution in the allochthonous complexes of NW Iberia (Galicia) and a WNW-ESE oriented general cross-section. The map shows the synformal structure of the complexes where a rootless branch of the main Pangea suture in Europe is exposed. The Somozas Mélange is a thick tectonic mixing unit located in the leading edge of the pile composed of exotic allochthonous units. The location of the geological map presented in Figure 3 is also shown.

Fig. 2.- Distribución de terrenos en los complejos alóctonos del NW de Iberia (Galicia), y sección geológica general de orientación WNW-ESE. El mapa muestra la estructura sinformal de los complejos, que contienen una rama desenraizada de la sutura de Pangea en Europa. La Mélange de Somozas es una potente unidad de mezcla tectónica situada en el frente de avance de la pila compuesta por unidades alóctonas exóticas. Se indica también la situación del mapa geológico de la Figura 3.

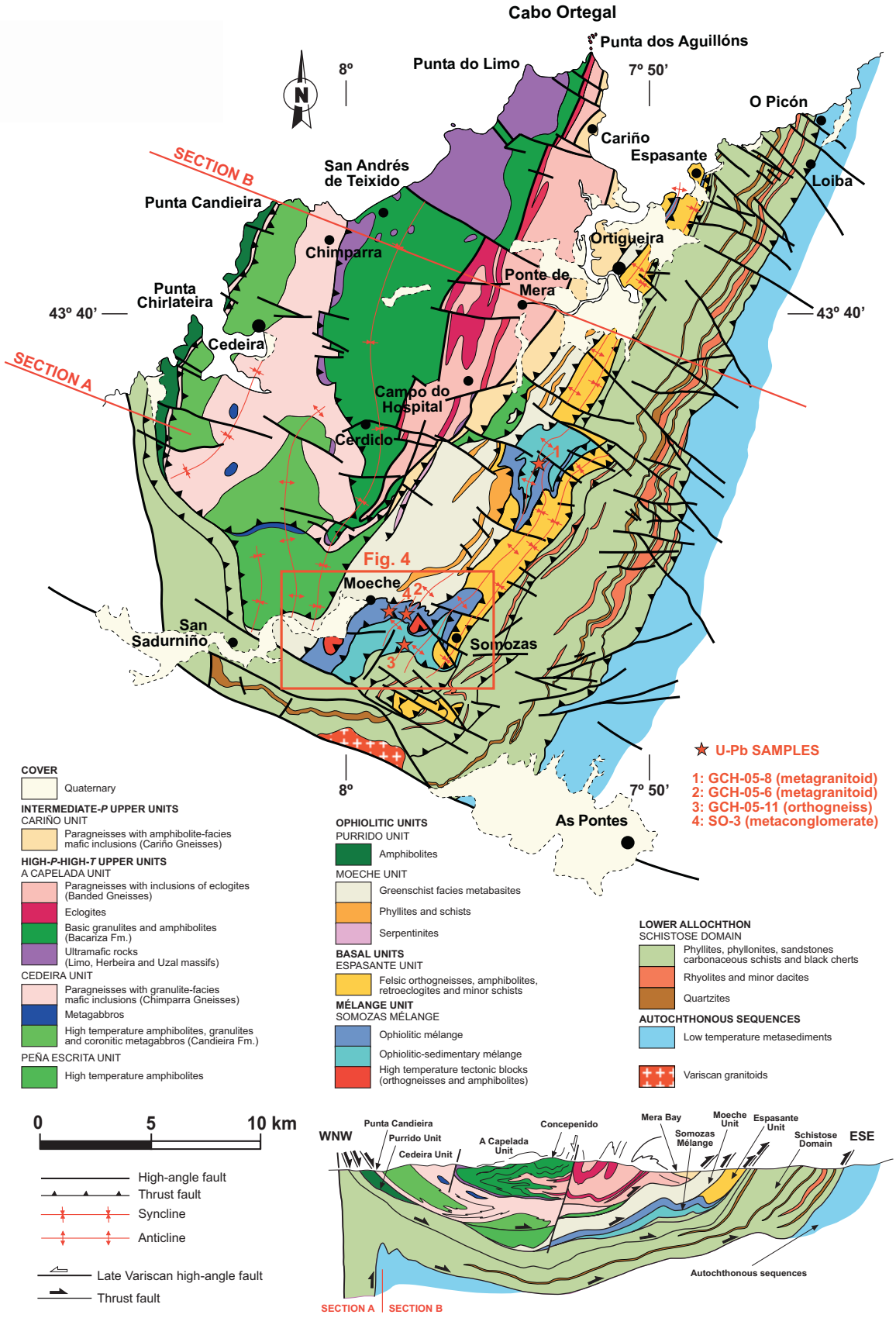

Fig. 3.- Geological map and cross-section of the Cabo Ortegal Complex. The location of the samples dated by U-Pb (stars) and the region of the Somozas Mélange mapped out in detail (rectangle) are also shown.

Fig. 3.- Mapa geológico y sección transversal del Complejo de Cabo Ortegal. Se indican la posición de las muestras datadas por U-Pb (estrellas) y el sector de la Mélange de Somozas cartografiado en detalle (rectángulo).

higher detrital character of its sedimentary series and by the abundance of felsic volcanics. The chronology of the Schistose Domain may be different between regions, and its stratigraphy and structure are poorly known. However, recent paleontological and U-Pb geochronological data suggest an Early to Middle Ordovician age for the Schistose Domain located below the Cabo Ortegal Complex (Valverde-Vaquero *et al.*, 2005).

In the NW Iberian Massif, the Somozas Mélange is the only tectonic mélange identified to date. This mélange is similar to a typical serpentinite mélange where a mantle wedge is involved in the mixing unit, and its characteristic structural position at the base of the exotic terranes, allows us to consider this unit as an important feature of Variscan convergence and a local manifestation of the Pangea suture. The Somozas Mélange appears in the leading edge of the allochthonous pile of NW Iberia (Figs. 2 and 3), which advanced from West to East (present coordinates) (Martínez Catalán *et al.*, 2007). The mélange is located at the contact between the allochthonous terranes and the units of the Gondwana margin that do not show high-P metamorphism, which consequently were not subducted below the southern margin of Laurussia.

3. Structure and rock types of the mélange unit

Based on the discontinuous character of its lithologies at regional scale, the Somozas Mélange was firstly described as a fragmented ophiolite, (Arenas, 1985; Arenas *et al.*, 1986). Marcos *et al.* (2002) pointed out the equivalence of this unit with a tectonic mélange. This mélange crops out discontinuously in the eastern part of the Cabo Ortegal Complex, in the core of upright late antiforms (Figs. 2 and 3). The type section and the best exposures are located to the west of the Somozas village, where the mélange unit appears in the core of two antiforms. This region was mapped in detail to investigate the lithology and internal structure of the mélange (Fig. 4). The mélange unit underlies the Moeche and Espasante units (lower ophiolitic units and basal units, respectively), cutting the contact between both units at a high angle as can be observed in the western limb of the Somozas Antiform. The mélange unit gently dips to the west and disappears below the Cabo Ortegal Complex, with no more recurrences in the NW Iberian Massif. This is the unit with the lowest structural position in the allochthonous complexes, but its existence is limited to the leading edge of the allochthonous pile.

The Somozas Mélange contains two different subunits (Fig. 4). The upper unit has a rather variable thickness reaching up to 800 m to the South of the Moeche village, and can be classified as a typical ophiolitic mélange where a highly sheared matrix of serpentinites surrounds tectonic blocks and slices of variable size and continuity (Fig. 5). The smallest tectonic blocks are one metre or so in length. The largest blocks in the mélange are kilometers in length. The most common rocks in the mélange are gabbros, diabases, granitoids and volcanic rocks. Large tectonic blocks of high temperature metamorphic rocks also occur. Moreover, intercalations of phyllites and phyllonites occur, whereas tectonic blocks and slices of sandstones, conglomerates and marbles are less common (Fig. 4). The lower subunit may attain thickness of 1000 m and is a mélange with a matrix of ocher-colored phyllites or blue phyllonites surrounding tectonic blocks and slices of the lithologies involved in the ophiolitic mélange. This subunit was formed later than the ophiolitic mélange and it represents a complex imbrication zone between the ophiolitic mélange and a metasedimentary unit. The entire Somozas Mélange is thrust over the Schistose Domain and hence is emplaced over series that belong to the external Gondwanan margin.

The igneous rocks involved in the Somozas Mélange do not generally preserve their primary mineralogy. Only a few rare metagabbros contain igneous clinopyroxene and orthopyroxene partially replaced by hornblende. The igneous phases are replaced by low temperature, or more rarely medium temperature, metamorphic minerals, developing mineral assemblages typical of the greenschist or amphibolite facies. This alteration was hydrothermal in origin, with an almost perfect preservation of the original igneous textures in areas where subsequent deformation was weak. The pervasive deformation inside the tectonic blocks and slices is very heterogeneous because the serpentinite matrix is preferentially sheared and this feature favors a low internal deformation in many of the large tectonic blocks and slices. The deformation and regional metamorphism associated with mélange formation and its later thrusting affect igneous rocks that previously underwent oceanic hydrothermal metamorphism.

The submarine volcanic rocks include lava flows, broken pillow breccias, submarine breccias, close-packed pillow lavas and hyaloclastites. The textures and the original mineralogy deduced from the hydrothermal phases, suggest basaltic and basaltic andesite compositions. The porphyritic types are abundant and contain many millimetre-sized pseudomorphs of plagioclase phenocrysts and less common pseudomorphs of mafic phenocrysts, all of them comprised of hydrothermal phases. The broken pillow breccias can include complete and undeformed pillow lavas up to 1 m in diameter, with chilled margins and blastoporphyritic cores. The submarine breccias can

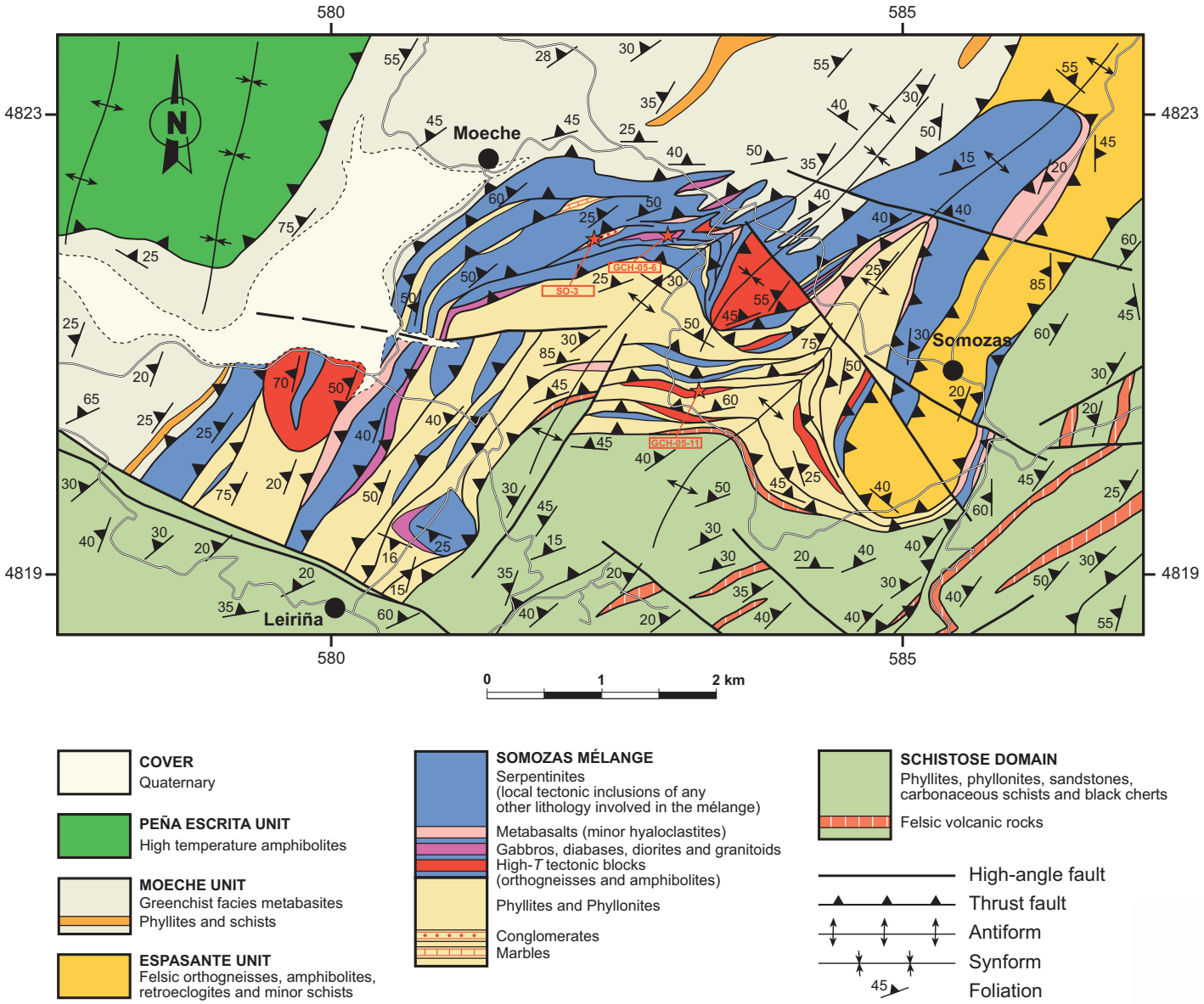

Fig. 4.- Geological map of the Somozas Mélange in the type locality around Somozas-Moeche. The mélange crops out in the core of a late antiform, where many tectonic slices of varied lithologies appear. The map includes the detailed location of the U-Pb samples picked up in this sector.

Fig. 4.- Mapa geológico de la Mélange de Somozas en la localidad tipo de los alrededores de Somozas-Moeche. La mélange aflora en el núcleo de una antiforma tardía, donde aparecen muchas escamas tectónicas de variable composición. El mapa indica también la posición detallada de las muestras para U-Pb recogidas en este sector.

show a variably recrystallized dark hyaloclastitic matrix, that in scarce outcrops may preserve remnants of shards. The volcanic rocks are intruded by abundant diabase dykes, but primary contacts with plutonic or sedimentary rocks are not exposed. Coarse to medium grained gabbros can appear both in monolithological slices or showing intrusive relationships with granitoids and diabases. The granitoids are fine to medium grained with well preserved primary textures, with compositions of diorites, quartz-diorites, tonalites and granodiorites. K-feldspar bearing types are almost absent, but there is a single tectonic block consisting of a K-feldspar-rich granitoid with a monzogranitic composition. In the metagranitoids, the primary plagioclase is typically replaced by albite and epidote-clinozoisite, whereas the primary mafic minerals are replaced by chlorite, amphibole or brown (or more rarely) green stilpnomelane. Highly sheared serpentinites are the most abundant rock type in the ophiolitic mélange, they seldom preserve primary igneous minerals but the presence of a chromium-rich spinel is almost pervasive.

The high temperature tectonic blocks contain a diversity of highly sheared tonalitic orthogneisses and meta-

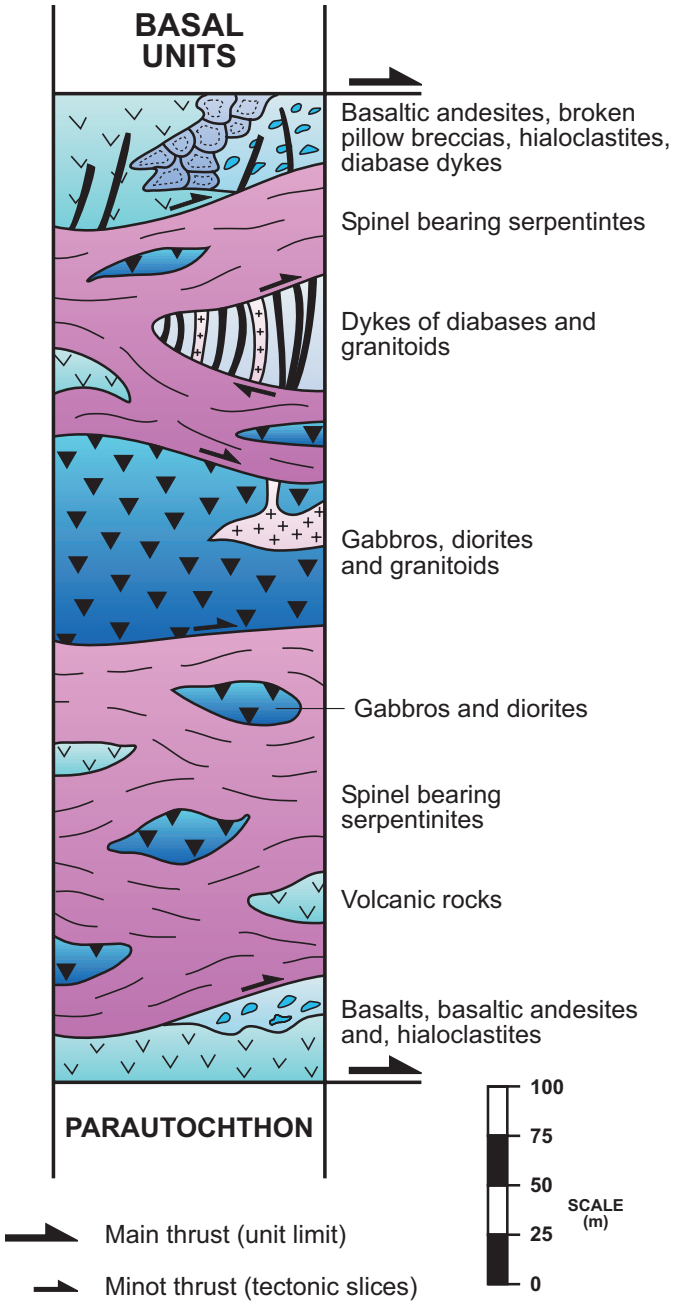

Fig. 5.- Idealized column showing the lithological constitution of the upper part of the Somozas Mélange which can be interpreted as a typical ophiolitic mélange.

Fig. 5.- Columna idealizada del conjunto litológico superior de la Mélange de Somozas, que puede interpretarse como una típica mélange ofiolítica.

basites. The metabasic rocks include common amphibolites and zoisite and rutile-rich amphibolites. There are no precise thermobarometric data for these rocks, but they contain characteristic types of amphiboles and a degree of recrystallization that enables their distinction from the other mafic igneous rocks involved in the mélange. The presence of tectonic blocks with contrasted metamorphic conditions is common in many large ophiolitic mélanges (Federico *et al.*, 2007). However, as discussed below, the protolith age obtained with U-Pb geochronology in one of the high-T orthogneisses suggests the correlation of these rocks with those of the basal units of the allochthonous complexes, probably with the Espasante Unit, rather than with the igneous rocks involved in the mélange. Therefore, it is suggested that these high-T rocks were incorporated to the mélange as metamorphic rocks derived from a terrane accreted in an upper position in the orogenic wedge.

As it is the case in other ophiolitic mélange, the tectonic blocks involved in the Somozas Mélange have a contrasting metamorphic evolution. Most of them exhibit greenschist facies mineral assemblages, whereas some metagabbros exhibit a mineralogy characteristic of the low-T part of the amphibolite facies (Arenas, 1985). Moreover, the metahyaloclastitic matrix of some submarine breccias contains paragonite, garnet and kyanite, and fragments in the breccia itself may contain almandine garnet growing around ilmenite aggregates. These data confirm the inclusion in the ophiolitic mélange of tectonic blocks derived from different depths, some of them with a metamorphic evolution probably developed under a high-P gradient, which is consistent with the generation of the tectonic mélange in a subduction zone.

The most abundant metasediments in the mélange are black or dark-blue phyllonites. Moreover, there are also common ocher-colored phyllites that may appear with a fine schistosity previous to the generation of the mélange. These metasediments are considered as tectonic blocks and slices that escaped from the strong shearing associated with mélange formation. Tectonic blocks of sandstones, conglomerates and marbles also occur. The tectonic blocks of metacarbonates have a thickness ranging between 1 m and tens of metres. The metacarbonates have a saccharoidal texture, are white to grey in colour and are intensely deformed. However, Van der Meer Mohr (1975) described some fauna that suggest an age that is younger than Middle Ordovician. Conglomerates and marbles similar to those included in the Somozas Mélange have not been described neither in the Parautochthonous series nor in other units of the allochthonous complexes. Hence, it is clear that they have exotic nature and uncertain origin. Moreover, a direct correlation between the pelitic metasediments in the Somozas Mélange and the metasediments from the upper part of the Parautochthonous below the Cabo Ortegal Complex cannot be established. In this way, it can be pointed out that on top of the Parautochthon several levels of high-silica rhyolites are observed, while their presence inside the Somozas Mélange has not been proven (Fig. 4).

4. U-Pb zircon geochronology

4.1. Sample selection and analytical techniques

In order to determine the age of the igneous and sedimentary lithologies involved in the Somozas Mélange, U-Pb zircon dating has been performed on 4 representative samples: one orthogneiss from a large high-T tectonic block (sample GCH-05-11); two metagranitoids involved in the ophiolitic mélange (samples GCH-05-8 and GCH-05-6); and one conglomerate also included in the ophiolitic mélange (sample SO-3). The location of these samples is shown in the map of the Cabo Ortegal Complex (Fig. 3). The detailed map of the Somozas Antiform (Fig. 4) also shows the location of the three samples coming from that region.

Sample GCH-05-11 is a tonalitic orthogneiss collected in the small village of Gradoy. It belongs to a tectonic block of orthogneisses included between phyllonites in the lower mélange subunit (Fig. 4). It is a medium grained orthogneiss with a cataclastic fabric that apparently developed after an earlier fabric of granoblastic character, and consists of quartz, albitic plagioclase, biotite, chlorite, sericite, epidote-clinozoisite, ilmenite, pyrite, apatite and zircon. The cataclasis occurred at medium temperature, during the retrogression of a previous mineral assemblage developed at higher temperature.

Sample GCH-05-8 is a barely deformed metagranitoid from the Insua region. It belongs to a tectonic block that includes granitoids, gabbros and diorites which appears surrounded by phyllites and phyllonites. The intrusive relationships between the igneous lithologies of this tectonic block are not clear. The metagranitoid dated by U-Pb geochronology has tonalitic composition, shows a fine grained granular texture and it is affected by a low-T metamorphism. The mineral composition is quartz, albitic plagioclase, chlorite, stilpnomelane, white mica, epidote-clinozoisite, ilmenite, pyrite, apatite and zircon.

Sample GCH-05-6 is a metagranitoid collected in the small village of Ferreiras. It is part of a monolithologic tectonic block included in serpentinites with hundred of meters-size continuity (Fig. 4). It is a medium grained, moderately deformed rock with blastogranular texture and monzogranitic composition. Contains quartz, plagioclase, K-feldspar, biotite, chlorite, white mica, epidote-clinozoisite, ilmenite, pyrite, apatite and zircon.

Sample SO-3 is a metaconglomerate collected near the little village of Ferreiras, in an old serpentinite quarry. It is part of a 7 m thick tectonic block included between mylonitic serpentinites (Fig. 4). The metaconglomerate is poorly deformed and contains cm-size pebbles of sandstones, pelites, cherts, limestones, plutonic rocks (quartz-diorites, tonalites and granitoids) and volcanic rocks (basalts, andesites, dacites and glass fragments). This metaconglomerate shows a low temperature (greenschist facies) metamorphic recrystallization.

U-Th-Pb analyses of zircon in samples GCH-05-11 and GCH-05-8 were conducted on the Bay SHRIMP-RG (Sensitive High Resolution Ion Microprobe-Reverse Geometry) operated by the SUMAC facility (USGS-Stanford University) during two analytical sessions in February and October 2006. Zircon separation was carried out at the Universidad Complutense (Madrid) following standard techniques, including crushing, pulverizing, Wilfley table, sieving, magnetic separator and methylene iodide. The zircons were handpicked under a binocular microscope and mounted on a double-sided adhesive on glass slides in 1 x 6 mm parallel rows together with some chips of zircon standard R33 (Black *et al.*, 2004). After being set in epoxy resin, the zircons were ground down to expose their central portions by using 1500 grit wet sandpaper, and polished with 6 μm and 1 μm diamond abrasive on a lap wheel. Prior to isotopic analysis, the internal structure, inclusions, fractures and physical defects were identified with transmitted and reflected light on a petrographic microscope, and with cathodoluminescence (CL) on a JEOL 5800LV electron microscope (housed at USGS-Denver). After the analysis, secondary electron images were taken to locate the exact position of the spots. Analytical procedures for zircon dating followed the methods described in Williams (1997). Secondary ions were generated from the target spot with an O^{2-} primary ion beam varying from 4-6 nA. The primary ion beam produced a spot with a diameter of ~25 microns and a depth of 1-2 microns for an analysis time of 8-10 minutes. Twelve peaks were measured sequentially in a single collector: $^{90}Zr_2{}^{16}O$, ^{204}Pb, background (0.050 mass units above ^{204}Pb), ^{206}Pb, ^{207}Pb, ^{208}Pb, ^{238}U, $^{248}Th^{16}O$, $^{254}U^{16}O$, $^{166}Er^{16}O$, $^{172}Yb^{16}O$, $^{180}Hf^{16}O$. One additional peak was included in the second session (^{155}Gd). Five scans were collected, and the counting time for ^{206}Pb was increased according to the Paleozoic age of the samples to improve counting statistics and precision of the $^{206}Pb/^{238}U$ age. Before collecting the data, the primary beam was rastered for 90-120 seconds over the area to be analyzed. The concentration of U was calibrated using zircon standard CZ3 (550 ppm U; Pidgeon *et al.*, 1995), and isotopic compositions were calibrated against R33 ($^{206}Pb^*/^{238}U$ = 0.06716, equivalent to an age of 419 Ma, Black *et al.*, 2004) which was analyzed every four analyses. Data reduction follows the methods described by Williams (1997), and Ireland and Williams (2003), and SQUID

(version 1.08) and ISOPLOT (version 3.00) software (Ludwig, 2002, 2003) were used. All the ages, except one, are younger than 1 Ga, so they are reported based on $^{206}Pb/^{238}U$ ratios corrected from common Pb using the ^{207}Pb method. The oldest age is reported based on its ^{204}Pb-corrected $^{206}Pb/^{207}Pb$ isotopic ratio. The Pb composition used for initial Pb corrections ($^{204}Pb/^{206}Pb$=0.0554, $^{207}Pb/^{206}Pb$=0.864 and $^{208}Pb/^{206}Pb$=2.097) was estimated using the Stacey and Kramers (1975) model. Analytical results are presented in Tables 1 and 2.

U-Th-Pb analyses of zircon in sample GCH-05-6 were conducted at the Natural History Museum of London using the analytical technique of laser ablation inductively coupled plasma mass spectrometry (LA-ICP-MS) during one analytical session in September 2005. Zircon separation was carried out at the Universidad Complutense (Madrid) following the standard techniques described in the previous samples. Zircons were set in synthetic resin mounts, polished and cleaned in a HNO_3 ultrasonic bath and polished to expose equatorial sections. Analytical instrumentation, analytical protocol and techniques, data reduction, age calculation and common Pb correction are as described by Jeffries *et al.* (2003). Concordia age calculations, and creation of concordia plots, were performed by using ISOPLOT (version 3.00) software (Ludwig, 2003). Analytical results are presented in Table 3.

U-Th-Pb analyses of zircon in sample SO-3 were conducted at the GEMOC Key Centre, Macquarie University, using a UV laser ablation system (Norman *et al.*, 1996) coupled to an Agilent 4500, Series 300 ICP-MS. Zircon separation was carried out at the Universidad Complutense (Madrid) following the standard techniques described in the previous samples. ICP-MS operating conditions, data acquisition parameters, analytical protocol and data processing methodology are the same as those specified by Martínez Catalán *et al.* (2008). Concordia age calculations, and creation of concordia plots, were performed by using ISOPLOT (version 3.00) software (Ludwig, 2003). Analytical results are presented in Table 4.

4.2. U-Pb results

Sample GCH-05-11 (Gradoy orthogneiss)

Zircons from sample GCH-05-11 are small, blocky, idiomorphic grains with light yellow color. Under cathodoluminescence (Fig. 6a), broad homogeneous weakly luminescent areas are evident in most of the cores. These areas are mantled by variably thick oscillatory zones that are separated by thin luminescent bands, suggesting different stages of zircon precipitation during the evolution of the magma (Corfu *et al.*, 2003). Some discontinuous non-luminescent rims can also be observed.

Twenty-three analyses performed in 21 zircon grains from the Gradoy orthogneiss were aimed either at homogeneous areas or at oscillatory zones, and only one non-luminescent rim was thick enough to place a spot. Excluding the seven oldest analyses based on their reverse discordance (analyses 14.1, 15.1, 15.2 and 16.1) or high common Pb (analyses 5.1, 5.2 and 6.1), and the six youngest due to Pb loss, a weighted mean $^{206}Pb/^{238}U$ age of 485 ± 6 Ma is obtained, with a mean square of weighted deviation (MSWD) of 1.6 (Fig. 7). This age is interpreted as the best estimate for the crystallization of the igneous protolith of the orthogneiss.

Sample GCH-05-8 (Insua granitoid)

In sample GCH-05-8, zircons are mainly colorless, clear, euhedral prismatic grains and broken prisms with preserved faces. Some tan, clear, and subrounded to multifaceted equant grains, typical of metamorphic environments (Corfu *et al.*, 2003) are present. CL images show different internal textures in the zircons, disregarding their morphology (Fig. 6b). Zircons with a homogeneous domain are poorly luminescent and are commonly surrounded by thin irregular non-luminescent rims. Some cores have luminescent oscillatory zoning, bordered by irregular, thin rims. Other zircons display complex internal structures with combined oscillatory and sector-zoned cores variably resorbed and mantled by a luminescent domain, which can be in turn surrounded by a discontinuous non-luminescent rim.

The forty-four analyses carried out in 40 grains from the Insua granitoid are divided according to their age into inherited, magmatic and Variscan. The inherited age population includes all the analyses older than 505 Ma. The oldest age corresponds to a rim in a rounded grain (28.1) that yields a discordant (15%) $^{207}Pb/^{206}Pb$ age of 2264 ± 22 Ma. Another individual analysis from a moderately luminescent core (29.1) yields a $^{206}Pb/^{238}U$ age of 772 ± 9 Ma. In grain 35.1, an age of 630 Ma is obtained, but this result has been rejected due to the high common Pb content. Two analyses from weakly luminescent oscillatory cores give ages of 568 and 567 Ma. Four of the six youngest ages in the inheritance population are obtained from non-luminescent cores and rims, and are rejected due to their high U content (U>2100 ppm, grains 12.1, 17.1 and 25.2) or high common Pb (>0.50%, analysis 40.2). Two remaining analyses from luminescent cores yield an age of 506 ± 2 and 510 ± 3 Ma (grains 23.1 and 34.1, respectively). The magmatic age population comprises 28 analyses ranging from 465 to 505 Ma. The five

TABLE 1.- SHRIMP U-Th-Pb ANALYSES OF ZIRCONS FROM THE GRADOY ORTHOGNEISS GCH-05-11

GCH-05-11 Anal. #		Common ^{206}Pb (%)	U (ppm)	Th (ppm)	$^{232}Th/^{238}U$	Isotopic ratios and 1σ (absolute) errors										$^{206}Pb/^{238}U$[d] age (Ma)	
						$^{238}U/^{206}Pb$[a]	±1σ	$^{207}Pb/^{206}Pb$[a]	±1σ	$^{238}U/^{206}Pb$[b]	±1σ	$^{207}Pb/^{206}Pb$[b]	±1σ	$^{206}Pb/^{238}U$[c]	±1σ		
21.1		0.449	1408	492	0.36	18.03137	1.41	0.05703	0.95	18.04867	1.41	0.05626	1.11	0.0552	0.0008	346	5
17.1		0.068	1209	473	0.40	14.41643	1.42	0.05604	0.91	14.42345	1.42	0.05564	0.98	0.0693	0.0010	432	6
20.1		0.186	643	211	0.34	14.31522	1.40	0.05706	1.22	14.31522	1.40	0.05706	1.22	0.0697	0.0010	435	6
1.1		0.138	1154	381	0.34	14.17749	1.38	0.05678	0.88	14.18240	1.38	0.05650	0.90	0.0704	0.0010	439	6
18.1		0.067	314	73	0.24	13.83705	1.51	0.05647	1.79	13.83705	1.51	0.05647	1.79	0.0722	0.0011	450	7
8.1		0.096	841	274	0.34	13.82558	1.40	0.05671	1.00	13.82558	1.40	0.05671	1.00	0.0723	0.0010	450	6
19.1		0.276	597	165	0.29	13.10161	1.40	0.05876	1.17	13.12878	1.40	0.05708	1.56	0.0761	0.0011	473	6
12.1		<0.001	417	97	0.24	13.08823	1.58	0.05622	1.47	13.10068	1.58	0.05544	1.56	0.0764	0.0012	475	7
2.1		<0.001	1457	482	0.34	13.00829	1.36	0.05657	0.74	13.01165	1.36	0.05636	0.77	0.0769	0.0011	477	6
9.1		0.142	726	210	0.30	12.89165	1.39	0.05788	1.05	12.89607	1.39	0.05760	1.08	0.0775	0.0011	481	7
4.1		0.027	1566	530	0.35	12.77682	1.36	0.05706	0.72	12.78078	1.36	0.05681	0.74	0.0782	0.0011	486	6
3.1		0.041	1418	509	0.37	12.74427	1.36	0.05721	0.75	12.74743	1.36	0.05701	0.78	0.0784	0.0011	487	6
7.1		0.009	1607	667	0.43	12.74628	1.36	0.05695	0.79	12.74628	1.36	0.05695	0.79	0.0784	0.0011	487	6
13.1		<0.001	1012	277	0.28	12.61773	1.37	0.05662	0.89	12.62259	1.37	0.05631	0.96	0.0793	0.0011	492	7
10.1		<0.001	550	149	0.28	12.53871	1.40	0.05629	1.19	12.53871	1.40	0.05629	1.19	0.0798	0.0011	495	7
11.1		<0.001	979	314	0.33	12.47006	1.37	0.05590	0.88	12.47006	1.37	0.05590	0.88	0.0803	0.0011	498	7
16.1		<0.001	845	263	0.32	11.97462	1.38	0.05705	0.94	11.97462	1.38	0.05705	0.94	0.0836	0.0012	517	7
5.1	R	0.340	797	245	0.32	11.88454	1.38	0.06048	0.94	11.93829	1.38	0.05682	1.72	0.0839	0.0012	519	7
14.1		<0.001	598	201	0.35	11.64601	1.40	0.05751	1.12	11.64601	1.40	0.05751	1.12	0.0859	0.0012	531	7
5.2	C	1.135	1101	364	0.34	11.31620	1.39	0.06751	1.89	11.46819	1.41	0.05670	5.10	0.0874	0.0012	540	7
6.1		0.749	1418	413	0.30	11.12346	1.40	0.06467	0.73	11.22166	1.40	0.05753	2.31	0.0892	0.0013	551	8
15.2	C	<0.001	1747	738	0.44	11.15173	1.36	0.05727	0.70	11.15415	1.36	0.05709	0.71	0.0898	0.0012	555	7
15.1	R	<0.001	2999	847	0.29	10.92881	1.35	0.05764	0.48	10.94201	1.35	0.05665	0.78	0.0916	0.0013	565	7

[a] Uncorrected ratios.
[b] Radiogenic lead ^{204}Pb corrected for common lead.
[c] Radiogenic lead ^{207}Pb corrected for common lead
[d] ^{207}Pb corrected for common lead.

Table 1.- U-Th-Pb SHRIMP analytical data for zircons from the orthogneiss GCH-05-11. C, core; R, rim. All errors are 1σ.
Tabla 1.- Datos analíticos U-Th-Pb (SHRIMP) de los circones del ortogneis GCH-05-11. C, centro; R, borde. Todos los errores son 1σ.

TABLE 2.- SHRIMP U-Th-Pb ANALYSES OF ZIRCONS FROM THE INSUA GRANITOID GCH-05-8

GCH-05-5 Anal. #		Common ^{206}Pb (%)	U (ppm)	Th (ppm)	$^{232}Th/^{238}U$	Isotopic ratios and 1σ (absolute) errors										$^{206}Pb/^{238}U^{d}$ age (Ma)	
						$^{238}U/^{206}Pb^{a}$	±1σ	$^{207}Pb/^{206}Pb^{a}$	±1σ	$^{238}U/^{206}Pb^{b}$	±1σ	$^{207}Pb/^{206}Pb^{b}$	±1σ	$^{206}Pb/^{238}U^{c}$	±1σ		
37.1		1.802	256	77	0.31	21.06184	0.92	0.06666	1.90	21.28388	1.06	0.05835	7.78	0.0466	0.0005	294	3
20.1		2.561	317	240	0.78	20.09512	0.81	0.07303	2.15	20.72375	0.99	0.04854	12.02	0.0485	0.0004	305	3
31.1		0.400	241	74	0.32	20.27289	0.91	0.05576	2.65	20.36914	0.92	0.05196	3.79	0.0491	0.0005	309	3
7.1		0.340	119	167	1.46	20.21830	1.26	0.05530	2.79	20.37535	1.29	0.04907	6.04	0.0493	0.0006	310	4
7.2		0.198	1811	7	0.00	19.79708	0.41	0.05432	0.90	19.84915	0.41	0.05221	1.59	0.0504	0.0002	317	1
11.1		0.340	135	123	0.94	13.33790	1.06	0.05907	2.11	13.38147	1.08	0.05643	3.95	0.0747	0.0008	465	5
27.1		0.419	1252	327	0.27	12.95107	0.33	0.06004	0.63	12.99535	0.34	0.05727	1.39	0.0769	0.0003	478	2
1.1	C	0.074	792	111	0.14	12.97634	0.42	0.05726	0.83	12.98183	0.42	0.05692	0.98	0.0770	0.0003	478	2
37.1		1.802	256	77	0.31	21.06184	0.92	0.06666	1.90	21.28388	1.06	0.05835	7.78	0.0466	0.0005	294	3
1.2	R	2.484	3657	733	0.21	12.45275	0.47	0.07703	0.71	12.74303	0.52	0.05857	5.03	0.0783	0.0005	486	3
32.1		0.152	137	45	0.34	12.61519	1.02	0.05822	2.00	12.67712	1.04	0.05424	3.82	0.0791	0.0008	491	5
4.1		0.175	1200	275	0.24	12.59997	0.34	0.05842	0.67	12.60974	0.35	0.05779	0.95	0.0792	0.0003	492	2
36.1		<0.001	632	96	0.16	12.61491	0.47	0.05644	0.92	12.64739	0.48	0.05434	1.77	0.0793	0.0004	492	2
24.2	R	0.189	1583	329	0.21	12.57869	0.33	0.05855	1.51	12.59759	0.33	0.05734	1.68	0.0793	0.0003	492	2
10.1		0.084	2173	525	0.25	12.58924	0.26	0.05770	0.51	12.58683	0.26	0.05786	0.53	0.0794	0.0002	492	1
39.1		0.004	713	97	0.14	12.58477	0.47	0.05707	1.05	12.58612	0.47	0.05698	1.13	0.0795	0.0004	493	2
19.1		0.117	2042	552	0.28	12.56269	0.27	0.05799	0.54	12.56532	0.27	0.05782	0.58	0.0795	0.0002	493	1
40.1	R	0.218	976	237	0.25	12.46358	0.40	0.05890	0.78	12.47296	0.40	0.05829	0.87	0.0801	0.0003	496	2
13.1		0.133	511	90	0.18	12.47165	0.53	0.05821	1.06	12.49534	0.53	0.05667	1.54	0.0801	0.0004	497	3
25.1	C	0.094	723	114	0.16	12.46407	0.45	0.05791	0.88	12.46063	0.45	0.05813	0.93	0.0802	0.0004	497	2
38.1		0.117	1105	220	0.21	12.45961	0.37	0.05809	0.93	12.47273	0.37	0.05724	1.01	0.0802	0.0003	497	2
18.1		<0.001	932	189	0.21	12.43954	0.40	0.05708	0.78	12.44179	0.40	0.05693	0.86	0.0804	0.0003	499	2

[a] Uncorrected ratios.
[b] Radiogenic lead ^{204}Pb corrected for common lead.
[c] Radiogenic lead ^{207}Pb corrected for common lead.
[d] ^{207}Pb corrected for common lead.

Table 2.- U-Th-Pb SHRIMP analytical data for zircons from the metagranitoid GCH-05-8. C, core; R, rim. All errors are 1σ. (Table 2 continues in next page)
Tabla 2.- Datos analíticos U-Th-Pb (SHRIMP) de los circones del metagranitoide GCH-05-8. C, centro; R, borde. Todos los errores son 1σ. (La Tabla 2 continúa en la página siguiente)

TABLE 2 (cont.).- SHRIMP U-Th-Pb ANALYSES OF ZIRCONS FROM THE INSUA GRANITOID GCH-05-8

GCH-05-5 Anal. #		Common ^{206}Pb (%)	U (ppm)	Th (ppm)	$^{232}Th/^{238}U$	Isotopic ratios and 1σ (absolute) errors										$^{206}Pb/^{238}U^{d}$ age (Ma)	
						$^{238}U/^{206}Pb^{a}$	±1σ	$^{207}Pb/^{206}Pb^{a}$	±1σ	$^{238}U/^{206}Pb^{b}$	±1σ	$^{207}Pb/^{206}Pb^{b}$	±1σ	$^{206}Pb/^{238}U^{c}$	±1σ		
14.1		0.357	408	71	0.18	12.39338	0.60	0.06009	1.17	12.41991	0.60	0.05835	1.69	0.0804	0.0005	499	3
15.1		<0.001	1822	477	0.27	12.42455	0.29	0.05711	0.56	12.42398	0.29	0.05715	0.56	0.0805	0.0002	499	1
16.1		0.122	827	142	0.18	12.39188	0.42	0.05820	0.83	12.39445	0.42	0.05803	0.85	0.0806	0.0003	500	2
30.1		0.457	834	149	0.18	12.34937	0.48	0.06092	1.52	12.41166	0.49	0.05684	2.32	0.0806	0.0004	500	2
21.1		<0.001	1275	358	0.29	12.40702	0.34	0.05650	0.68	12.41413	0.34	0.05603	0.71	0.0807	0.0003	500	2
9.1		0.291	1714	552	0.33	12.35538	0.31	0.05959	0.68	12.38251	0.32	0.05781	1.17	0.0807	0.0003	500	2
6.1		0.075	1609	231	0.15	12.37415	0.33	0.05784	0.63	12.39541	0.33	0.05645	0.95	0.0808	0.0003	501	2
24.1	C	0.020	658	83	0.13	12.36436	0.47	0.05742	0.92	12.36061	0.47	0.05766	0.98	0.0809	0.0004	501	2
8.1		<0.001	1687	360	0.22	12.36325	0.29	0.05709	0.57	12.36877	0.29	0.05673	0.59	0.0809	0.0002	502	1
22.1		1.138	377	66	0.18	12.19195	0.76	0.06654	1.44	12.35292	0.84	0.05593	5.87	0.0811	0.0006	503	4
26.1		0.105	135	54	0.41	12.29280	1.02	0.05817	2.01	12.25665	1.05	0.06056	4.02	0.0813	0.0009	504	5
23.1		0.111	671	85	0.13	12.22728	0.47	0.05829	0.91	12.21986	0.47	0.05878	0.91	0.0817	0.0004	506	2
40.2	C	0.616	820	126	0.16	12.15208	0.54	0.06240	0.88	12.22461	0.55	0.05758	2.22	0.0818	0.0005	507	3
17.1		0.002	2239	667	0.31	12.22667	0.27	0.05742	0.52	12.22528	0.27	0.05751	0.53	0.0818	0.0002	507	1
34.1		<0.001	564	36	0.07	12.14734	0.50	0.05722	0.98	12.14166	0.50	0.05760	0.97	0.0823	0.0004	510	3
12.1		<0.001	6105	2161	0.37	12.11794	0.18	0.05728	0.30	12.11794	0.18	0.05728	0.30	0.0825	0.0002	511	1
25.2	R	<0.001	2175	584	0.28	11.70491	0.31	0.05787	0.61	11.70922	0.31	0.05757	0.65	0.0854	0.0003	529	2
33.1		0.149	144	86	0.62	10.85459	0.95	0.06022	1.77	10.83532	0.95	0.06166	1.75	0.0920	0.0009	567	5
5.1		0.366	93	53	0.59	10.81721	1.19	0.06201	2.20	10.85283	1.23	0.05934	5.22	0.0921	0.0011	568	7
35.1		29.921	533	479	0.93	6.82647	0.53	0.30558	27.49	9.12257	11.73	-	-	0.1027	0.0163	630	95
29.1		0.127	74	20	0.27	7.85339	1.25	0.06597	2.09	7.86511	1.27	0.06474	3.42	0.1272	0.0017	772	9
28.1		3.197	268	106	0.41	2.80398	0.65	0.14503	1.18	2.81058	0.65	0.14304	1.27	0.3452	0.0031	2264	22

[a] Uncorrected ratios.
[b] Radiogenic lead ^{204}Pb corrected for common lead.
[c] Radiogenic lead ^{207}Pb corrected for common lead.
[d] ^{207}Pb corrected for common lead
* Except analysis 28.1 ($^{207}Pb/^{206}Pb$ age, ^{204}Pb corrected for common lead).

Table 2.- Cont.
Tabla 2.- Cont.

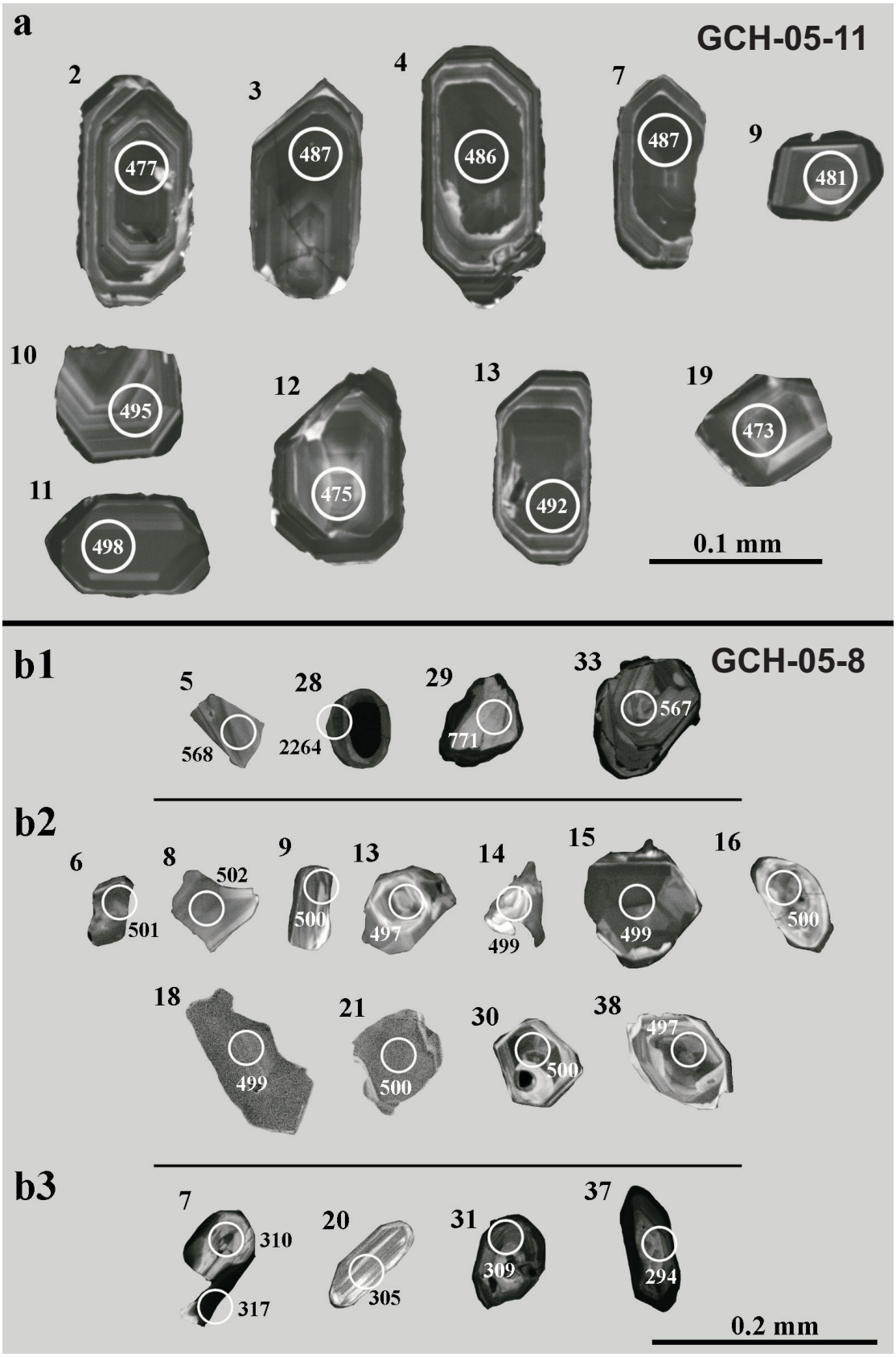

Fig. 6.- Cathodoluminescence images for selected zircons from samples GCH-05-11 (orthogneiss) and GCH-05-8 (metagranitoid). a) magmatic ages; b1) inheritance ages, b2) magmatic ages, b3) Variscan ages.

Fig. 6.- Imágenes de catodoluminiscencia de circones seleccionados de la muestras GCH-05-11 (ortogneis) y GCH-05-8 (metagranitoide): a) edades magmáticas; b1) edades heredadas, b2) edades magmáticas, b3) edades variscas.

TABLE 3.- LA-ICP-MS U-Pb ANALYSES OF ZIRCONS FROM THE FERREIRAS GRANITOID GCH-05-6.

Sample		Isotopic ratios and 1σ (absolute) errors						Ages and 2σ errors (Ma)						% disc
Anal. #	Th/U	$^{206}Pb/^{238}U$	±1σ	$^{207}Pb/^{235}U$	±1σ	$^{207}Pb/^{206}Pb$	±1σ	$^{206}Pb/^{238}U$	±2σ	$^{207}Pb/^{235}U$	±2σ	$^{207}Pb/^{206}Pb$	±2σ	
jl13b05	0.20	0.0832	0.0003	0.6522	0.0044	0.0569	0.0004	515	4	510	5	484	30	-6.40
jl13a10	0.23	0.0790	0.0007	0.6240	0.0062	0.0573	0.0005	490	8	492	8	500	40	2.00
jl13b16	0.24	0.0828	0.0006	0.6537	0.0056	0.0572	0.0004	513	7	511	7	500	30	-2.60
jl13b10	0.28	0.0841	0.0006	0.6638	0.0053	0.0573	0.0005	520	7	517	6	500	42	-4.00
jl13b13	0.27	0.0858	0.0004	0.6786	0.0043	0.0574	0.0003	530	4	526	5	504	26	-5.16
jl13a05	0.27	0.0822	0.0004	0.6513	0.0038	0.0575	0.0004	509	5	509	5	510	30	0.20
jl13d09	0.30	0.0881	0.0004	0.6990	0.0036	0.0576	0.0003	544	4	538	4	512	20	-6.25
jl13d13	0.29	0.0881	0.0008	0.6992	0.0050	0.0575	0.0003	544	10	538	6	512	22	-6.25
jl13a14	0.18	0.0773	0.0003	0.6148	0.0049	0.0577	0.0005	480	4	487	6	516	36	6.98
jl13c08	0.31	0.0854	0.0003	0.6802	0.0032	0.0577	0.0003	529	4	527	4	518	24	-2.12
jl13d07	0.28	0.0883	0.0004	0.7034	0.0030	0.0577	0.0003	546	5	541	4	518	20	-5.41
jl13a13	0.23	0.0803	0.0004	0.6398	0.0040	0.0578	0.0004	498	5	502	5	520	28	4.23
jl13a11	0.22	0.0859	0.0006	0.6848	0.0041	0.0578	0.0003	531	7	530	5	522	24	-1.72
jl13b14	0.27	0.0857	0.0009	0.6838	0.0079	0.0579	0.0005	530	10	529	10	524	36	-1.15
jl13c13	0.25	0.0858	0.0005	0.6852	0.0039	0.0579	0.0002	530	5	530	5	526	18	-0.76
jl13b15	0.25	0.0878	0.0005	0.7017	0.0054	0.0580	0.0003	542	6	540	6	528	22	-2.65
jl13b06	0.31	0.0894	0.0005	0.7152	0.0036	0.0580	0.0001	552	6	548	4	528	12	-4.55
jl13c05	0.24	0.0875	0.0008	0.7005	0.0056	0.0581	0.0003	541	9	539	7	530	26	-2.08
jl13b11	0.29	0.0827	0.0004	0.6629	0.0029	0.0581	0.0003	512	5	516	3	534	24	4.12
jl13a07	0.33	0.0843	0.0004	0.6754	0.0038	0.0581	0.0004	521	5	524	5	534	28	2.43
jl13d11	0.27	0.0883	0.0006	0.7079	0.0050	0.0581	0.0003	546	7	543	6	534	22	-2.25
jl13b07	0.23	0.0842	0.0006	0.6767	0.0077	0.0583	0.0007	521	7	525	9	538	54	3.16
jl13a12	0.24	0.0818	0.0005	0.6579	0.0051	0.0583	0.0004	507	6	513	6	540	28	6.11
jl13c15	0.26	0.0841	0.0006	0.6760	0.0051	0.0583	0.0003	521	7	524	6	540	22	3.52
jl13d14	0.25	0.0888	0.0007	0.7141	0.0055	0.0583	0.0002	548	9	547	6	540	20	-1.48
jl13c09	0.29	0.0881	0.0005	0.7091	0.0050	0.0584	0.0003	544	5	544	6	542	20	-0.37
jl13a06	0.24	0.0812	0.0003	0.6549	0.0054	0.0585	0.0004	503	4	512	7	548	32	8.21
jl13d15	0.27	0.0866	0.0008	0.6998	0.0064	0.0586	0.0003	536	9	539	8	550	20	2.55
jl13c10	0.22	0.0854	0.0007	0.6905	0.0057	0.0586	0.0004	528	9	533	7	552	30	4.35
jl13d12	0.32	0.0899	0.0007	0.7281	0.0063	0.0587	0.0003	555	8	555	7	556	18	0.18
jl13a16	0.26	0.0840	0.0004	0.6813	0.0033	0.0588	0.0003	520	4	528	4	560	20	7.14
jl13d06	0.28	0.0868	0.0005	0.7048	0.0041	0.0589	0.0003	537	6	542	5	562	24	4.45
jl13d16	0.26	0.0860	0.0007	0.7002	0.0073	0.0591	0.0004	532	9	539	9	568	32	6.34
jl13d10	0.26	0.0897	0.0004	0.7380	0.0056	0.0597	0.0003	554	5	561	7	592	24	6.42

disc%= percent discordance calculated from $^{207}Pb/^{206}Pb$ and $^{206}Pb/^{238}U$ ages (negative values: reversely discordant analyses).

Table 3. LA-ICP-MS U-Pb analyses of zircons from the metagranitoid GCH-05-6.
Tabla 3. Datos analíticos U-Pb (LA-ICP-MS) de los circones del metagranitoide GCH-05-6.

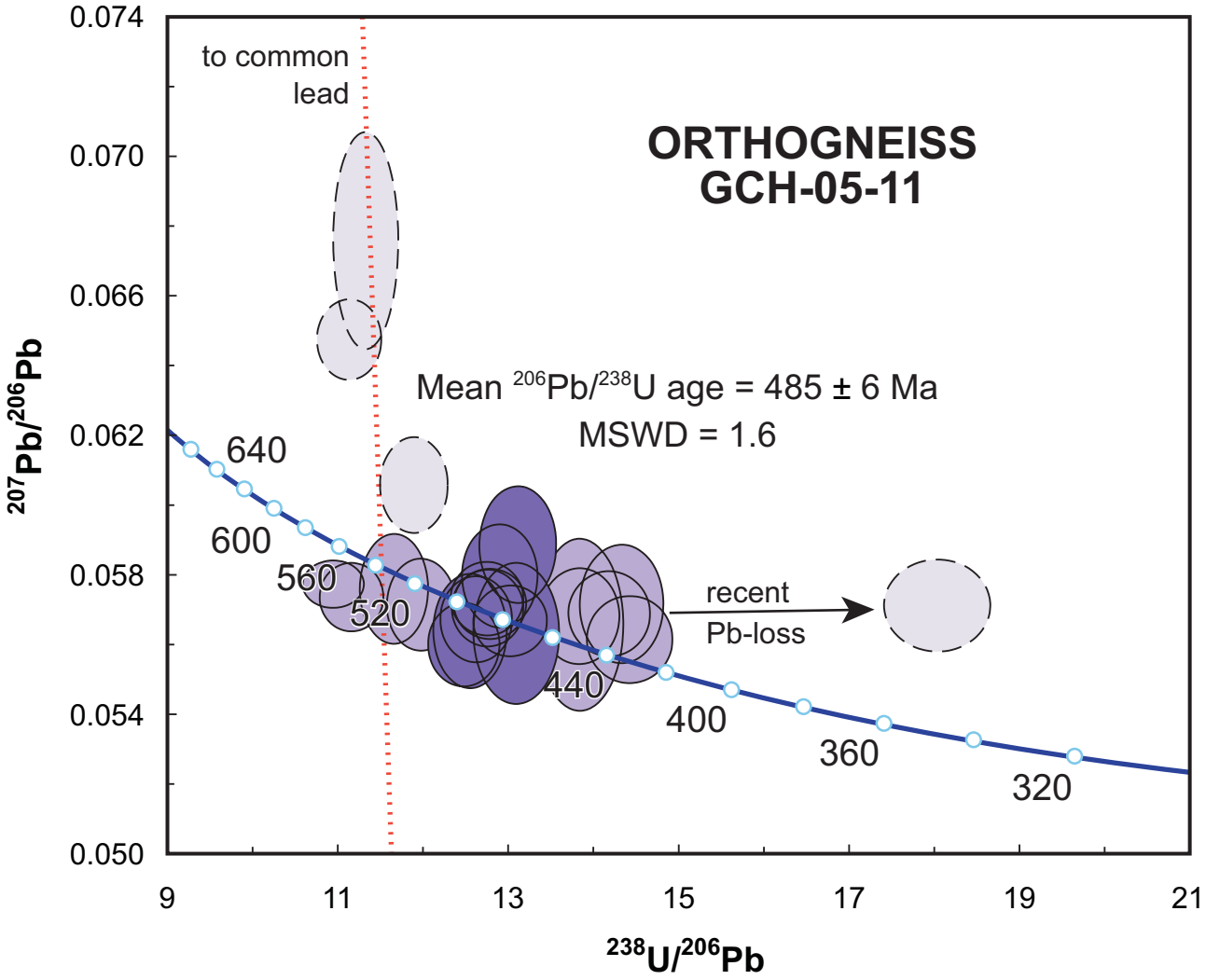

Fig. 7.- Tera-Wasserburg plot showing the distribution of SHRIMP zircon analyses from the orthogneiss GCH-05-11. Dark blue ellipses correspond to analyses considered to obtain the mean age; light blue ellipses represent discarded analyses; dashed ellipses stand for high common Pb analyses. Error ellipses are ± 2σ.

Fig. 7.- Diagrama de Tera-Wasserburg con la proyección de los circones analizados mediante SHRIMP en el ortogneis GCH-05-11. Las elipses de color azul oscuro corresponden a los análisis considerados para calcular la edad media; las elipses de color azul claro representan análisis descartados; las elipses discontinuas corresponden a análisis con elevado contenido en plomo común. Las elipses de error son ± 2σ.

youngest ages are rejected due to their high U content (analysis 1.2), high common Pb (analyses 1.2, 11.1 and 27.1), probable presence of inclusions (analyses 1.2 and 2.1) or mixed domains (analyses 1.1, 11.1 and 27.1). The next seven youngest analyses yield a mean age of 492 ± 1 Ma. However, these spots should be rejected due to the possibility of Pb loss because the secondary electron images taken after the SHRIMP session show that they hit small fractures that were not visible in the reflected light images used during the analytical session. Two older analyses are also discarded due to their big error (spot 26.1) and high common Pb (spot 22.1). The remaining 14 analyses in this population yield a mean age of 499 ± 1 Ma (MSWD = 0.79), which is considered the best estimate for the crystallization of this metagranitoid (Fig. 8).

The Variscan age population is constituted by five analyses that yield a mean age of 311 ± 11 Ma, with a MSWD of 16 (Fig. 8). This small number of analysis suggests that the Variscan ages could be the result of Pb loss. However, the possibility that this age could represent metamorphic zircon recrystallization or new zircon growth cannot be ruled out.

Sample GCH-05-6 (Ferreiras granitoid)

Forty-eight analyses were performed on 46 zircon grains from the granitoid sample GCH-05-6. Fourteen of those were rejected based on its discordance higher than 10%. The 34 selected analyses yielded $^{206}Pb/^{238}U$ ages ranging between 480 ± 4 and 555 ± 8 Ma (Table 3). When plotted in the concordia diagram, they constitute a con-

tinuous cluster, and it is possible to calculate a concordia age where there is maximum density of overlapping ellipses, obtaining a result of 527 ± 2 Ma (MSWD = 0.64; Fig. 9). The same result is also obtained by calculating the average age of the whole set of selected data. The features of the zircon crystals and their low Th/U ratios (0.18-0.33, see Table 3) are compatible with an igneous origin. Therefore, the Cambrian age obtained for the U-Pb dating of this granitoid is interpreted as its protolith age.

Sample SO-3 (Ferreiras conglomerate)

Sixty analyses were performed in zircon grains from the sample SO-3, of which only concordant or nearly concordant (<10% discordant) data were considered for interpretation of detrital zircon age. U-Pb and Pb-Pb ratios and ages for the 59 selected analyses are given in Table 4. The reported ages used to plot the population histogram (Fig. 10b) are the $^{207}Pb/^{206}Pb$ ages for zircons older than 1.0 Ga and $^{206}Pb/^{238}U$ for those younger than 1.0 Ga. This is because $^{207}Pb/^{206}Pb$ ages become increasingly imprecise below 1.0 Ga due to the change of the concordia slope. The most important population of zircons (40.7% of the analyzed grains) is represented by 24 concordant and subconcordant analyses with U-Pb Middle Ordovician to Neoproterozoic ages ranging between 464 ± 7 and 628 ± 6 Ma (Table 4, Fig. 10), with the maximum density around 500 and 660 Ma. The second significant population is comprised of 15 concordant and subconcordant analyses with $^{207}Pb/^{206}Pb$ ages between 1842 ± 9 and 2075 ± 9 Ma, and the maximum density around 1900 and 2070 Ma. There are also a few clusters of analyses (16 in total) of Palaeoproterozoic and Archaean ages, three analyses of Mesoproterozoic ages ranging from 1209 ± 10 to 1366 ± 9 Ma and a single Neoproterozoic analysis of 708 ± 6 Ma (Table 4, Fig. 10).

The youngest zircon dated from this conglomerate sample is concordant with an age of 464 ± 7 Ma. Taking into account that this unit only developed low grade metamorphism it could be possible to interpret this datum as the maximum depositional age of the sediments. However

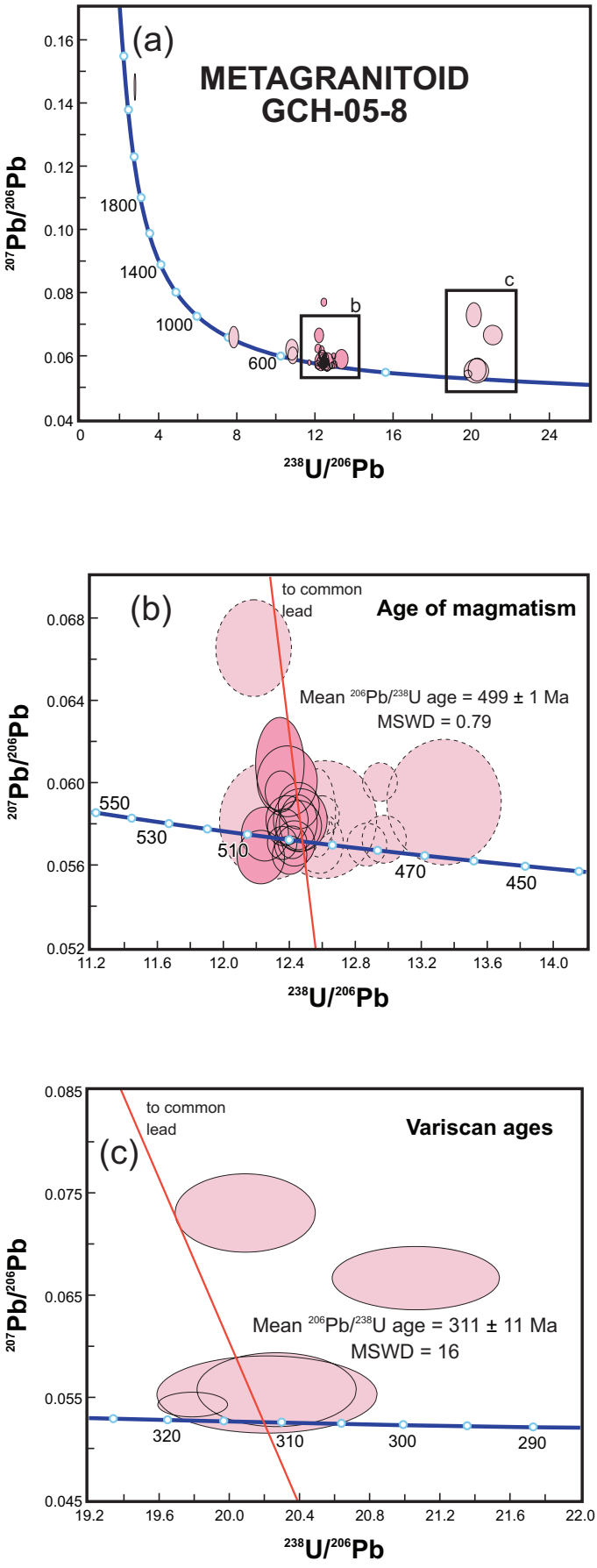

Fig. 8.- Tera-Wasserburg plot showing the distribution of SHRIMP zircon analyses from the metagranitoid GCH-05-8. a) all analyses; b) magmatic ages, dashed ellipses represent analyses not considered for the mean age; c) Variscan ages. Error ellipses are ± 2σ.

Fig. 8.- Diagrama de Tera-Wasserburg con la proyección de los circones analizados mediante SHRIMP en el metagranitoide GCH-05-8. a) todos los análisis; b) edades magmáticas, las elipses discontinuas corresponden a análisis no considerados para la edad media; c) edades variscas. Las elipses de error son ± 2σ.

TABLE 4.- LA-ICP-MS U-Pb ANALYSES OF DETRITAL ZIRCONS FROM THE FERREIRAS CONGLOMERATE SO-3.

Sample SO-3		Isotopic ratios and 1σ (absolute) errors						Ages and 1σ errors (Ma)						Reported age		
Anal. #	Th/U	$^{206}Pb/^{238}U$	±1σ	$^{207}Pb/^{235}U$	±1σ	$^{207}Pb/^{206}Pb$	±1σ	$^{206}Pb/^{238}U$	±1σ	$^{207}Pb/^{235}U$	±1σ	$^{207}Pb/^{206}Pb$	±1σ	Age (Ma)	±1σ	% disc
SO3-109	1.90	0.0746	0.0013	0.5802	0.036	0.0564	0.0036	464	7	465	23	469	110	464	7	1.1
SO3-111	1.78	0.0748	0.0010	0.5817	0.025	0.0564	0.0025	465	6	466	16	468	73	465	6	0.7
SO3-112	1.27	0.0775	0.0009	0.6103	0.022	0.0571	0.0021	481	6	484	14	497	57	481	6	3.2
SO3-110	1.88	0.0778	0.0009	0.6121	0.025	0.0571	0.0024	483	6	485	15	495	67	483	6	2.5
SO3-108	1.91	0.0784	0.0011	0.6178	0.030	0.0571	0.0029	487	7	488	19	496	83	487	7	2.0
SO3-14	0.18	0.0802	0.0009	0.6339	0.010	0.0573	0.0009	497	5	498	6	505	16	497	5	1.5
SO3-17	0.18	0.0809	0.0008	0.6387	0.007	0.0573	0.0007	501	5	502	4	503	10	501	5	0.4
SO3-33	0.15	0.0811	0.0008	0.6411	0.007	0.0574	0.0007	503	5	503	4	505	11	503	5	0.6
SO3-113	0.91	0.0816	0.0014	0.6458	0.033	0.0574	0.0030	506	8	506	20	507	81	506	8	0.2
SO3-43	0.20	0.0839	0.0008	0.6766	0.008	0.0585	0.0008	519	4	525	5	549	13	519	4	5.7
SO3-47	1.67	0.0864	0.0009	0.6926	0.019	0.0582	0.0016	534	6	534	11	536	40	534	6	0.3
SO3-53	0.63	0.0901	0.0009	0.7303	0.008	0.0588	0.0007	556	5	557	5	558	11	556	5	0.4
SO3-55	0.47	0.0914	0.0009	0.7422	0.009	0.0589	0.0007	564	5	564	5	564	12	564	5	0.0
SO3-39	0.94	0.0918	0.0009	0.7537	0.010	0.0596	0.0009	566	5	570	6	588	14	566	5	4.0
SO3-38	0.34	0.0922	0.0009	0.7503	0.008	0.0591	0.0007	568	5	568	5	569	11	568	5	0.1
SO3-35	0.74	0.0930	0.0010	0.7595	0.012	0.0593	0.0010	573	6	574	7	576	18	573	6	0.6
SO3-45	0.31	0.0931	0.0009	0.7651	0.010	0.0596	0.0008	574	6	577	6	588	13	574	6	2.5
SO3-37	0.59	0.0955	0.0009	0.7863	0.011	0.0597	0.0010	588	5	589	6	593	16	588	5	0.9
SO3-46	0.40	0.0958	0.0009	0.7871	0.009	0.0596	0.0008	590	6	590	5	590	12	590	6	0.1
SO3-106	0.55	0.0980	0.0010	0.8112	0.012	0.0600	0.0009	603	6	603	7	604	16	603	6	0.2
SO3-61	0.43	0.0993	0.0011	0.8242	0.014	0.0602	0.0011	610	6	610	8	612	19	610	6	0.3
SO3-22	0.45	0.1004	0.0009	0.8357	0.011	0.0604	0.0009	617	5	617	6	618	15	617	5	0.2
SO3-05	0.06	0.1020	0.0011	0.8560	0.011	0.0609	0.0008	626	6	628	6	635	12	626	6	1.5
SO3-54	0.17	0.1023	0.0011	0.8570	0.013	0.0607	0.0009	628	6	628	7	630	15	628	6	0.3
SO3-19	0.29	0.1161	0.0011	1.0083	0.011	0.0630	0.0007	708	6	708	6	708	10	708	6	0.0
SO3-48	0.55	0.2061	0.0019	2.2864	0.026	0.0805	0.0010	1208	10	1208	8	1209	10	1209	10	0.1
SO3-50	0.48	0.2308	0.0021	2.7418	0.034	0.0862	0.0012	1339	11	1340	9	1342	12	1342	12	0.2
SO3-16	0.74	0.2350	0.0022	2.8255	0.031	0.0872	0.0010	1360	12	1362	8	1366	9	1366	9	0.4
SO3-11	1.55	0.3306	0.0030	5.1321	0.054	0.1126	0.0014	1841	14	1841	9	1842	9	1842	9	0.0

disc%= percent discordance calculated from $^{207}Pb/^{206}Pb$ and $^{206}Pb/^{238}U$ ages.

Table 4.- LA-ICP-MS analyses of detrital zircons from the metaconglomerate SO-3. (Table 4 continues in next page)

Tabla 4.- Datos analíticos U-Pb (LA-ICP-MS) de los circones detríticos del metaconglomerado SO-3. (Esta tabla continúa en la página siguiente)

TABLE 4 (cont.)-- LA-ICP-MS U-Pb ANALYSES OF DETRITAL ZIRCONS FROM THE FERREIRAS CONGLOMERATE SO-3.

Sample SO-3		Isotopic ratios and 1σ (absolute) errors						Ages and 1σ errors (Ma)						Reported age		
Anal. #	Th/U	$^{206}Pb/^{238}U$	±1σ	$^{207}Pb/^{235}U$	±1σ	$^{207}Pb/^{206}Pb$	±1σ	$^{206}Pb/^{238}U$	±1σ	$^{207}Pb/^{235}U$	±1σ	$^{207}Pb/^{206}Pb$	±1σ	Age (Ma)	±1σ	% disc
SO3-04	1.70	0.3570	0.0032	6.0106	0.059	0.1221	0.0014	1968	15	1977	9	1988	8	1988	8	1.2
SO3-57	0.41	0.3361	0.0033	5.3084	0.086	0.1146	0.0021	1868	16	1870	14	1873	16	1873	16	0.3
SO3-56	0.73	0.3429	0.0032	5.5141	0.060	0.1166	0.0014	1901	15	1903	9	1905	9	1905	9	0.3
SO3-02	2.44	0.3436	0.0036	5.5324	0.075	0.1168	0.0017	1904	17	1906	12	1908	11	1908	11	0.3
SO3-42	1.13	0.3447	0.0032	5.5548	0.059	0.1169	0.0014	1909	15	1909	9	1909	9	1909	9	0.0
SO3-44	0.75	0.3452	0.0032	5.5701	0.060	0.1170	0.0014	1912	16	1911	9	1911	9	1911	9	0.0
SO3-58	0.44	0.3556	0.0039	5.9531	0.089	0.1214	0.0019	1961	18	1969	13	1977	13	1977	13	0.9
SO3-60	0.11	0.3670	0.0036	6.2812	0.072	0.1241	0.0016	2015	17	2016	10	2017	9	2017	9	0.1
SO3-06	0.63	0.3694	0.0035	6.3556	0.068	0.1248	0.0014	2026	17	2026	9	2026	8	2026	8	0.0
SO3-25	0.41	0.3772	0.0032	6.6281	0.062	0.1275	0.0014	2063	15	2063	8	2063	7	2063	7	0.0
SO3-31	0.48	0.3736	0.0034	6.5814	0.065	0.1278	0.0014	2046	16	2057	9	2068	8	2068	8	1.2
SO3-20	1.15	0.3778	0.0034	6.6559	0.071	0.1278	0.0016	2066	16	2067	9	2068	8	2068	8	0.1
SO3-28	1.25	0.3781	0.0034	6.6632	0.065	0.1278	0.0014	2067	16	2068	9	2068	8	2068	8	0.1
SO3-08	0.29	0.3797	0.0036	6.7175	0.070	0.1283	0.0014	2075	17	2075	9	2075	8	2075	8	0.0
SO3-01	0.52	0.3934	0.0039	7.3393	0.081	0.1353	0.0015	2138	18	2154	10	2168	9	2168	9	1.6
SO3-40	0.21	0.4172	0.0087	8.3279	0.291	0.1448	0.0054	2248	40	2267	32	2285	33	2285	33	2.0
SO3-107	0.36	0.4219	0.0040	8.6014	0.117	0.1479	0.0024	2269	18	2297	12	2321	29	2321	29	2.7
SO3-59	0.59	0.4496	0.0049	9.8997	0.156	0.1597	0.0026	2393	22	2425	15	2453	13	2453	13	2.9
SO3-51	0.78	0.4712	0.0046	10.5983	0.122	0.1632	0.0020	2489	20	2489	11	2489	9	2489	9	0.0
SO3-24	0.33	0.4833	0.0052	11.2217	0.149	0.1684	0.0023	2542	23	2542	12	2542	10	2542	10	0.0
SO3-52	0.70	0.4655	0.0051	10.8578	0.244	0.1692	0.0042	2464	23	2511	21	2550	43	2550	43	4.1
SO3-29	0.35	0.5055	0.0045	12.4415	0.119	0.1785	0.0019	2637	19	2638	9	2639	7	2639	7	0.1
SO3-18	0.58	0.5077	0.0045	12.6521	0.123	0.1808	0.0020	2647	19	2654	9	2660	7	2660	7	0.6
SO3-26	0.45	0.5170	0.0046	13.0905	0.124	0.1837	0.0020	2686	20	2686	9	2686	7	2686	7	0.0
SO3-09	0.56	0.5350	0.0051	14.1942	0.151	0.1924	0.0022	2763	22	2763	10	2763	8	2763	8	0.0
SO3-23	0.58	0.5502	0.0050	15.2761	0.145	0.2014	0.0021	2826	21	2833	9	2837	7	2837	7	0.5
SO3-21	0.15	0.5534	0.0058	15.4041	0.190	0.2019	0.0025	2839	24	2841	12	2842	9	2842	9	0.1
SO3-03	0.27	0.5547	0.0049	15.4649	0.151	0.2022	0.0023	2845	20	2844	9	2844	7	2844	7	0.0
SO3-07	0.52	0.5979	0.0053	18.6053	0.176	0.2257	0.0024	3021	21	3022	9	3022	7	3022	7	0.1
SO3-10	0.67	0.6541	0.0063	23.4129	0.250	0.2596	0.0029	3244	24	3244	10	3245	8	3245	8	0.0

Table 4.- Cont.
Tabla 4.- Cont.

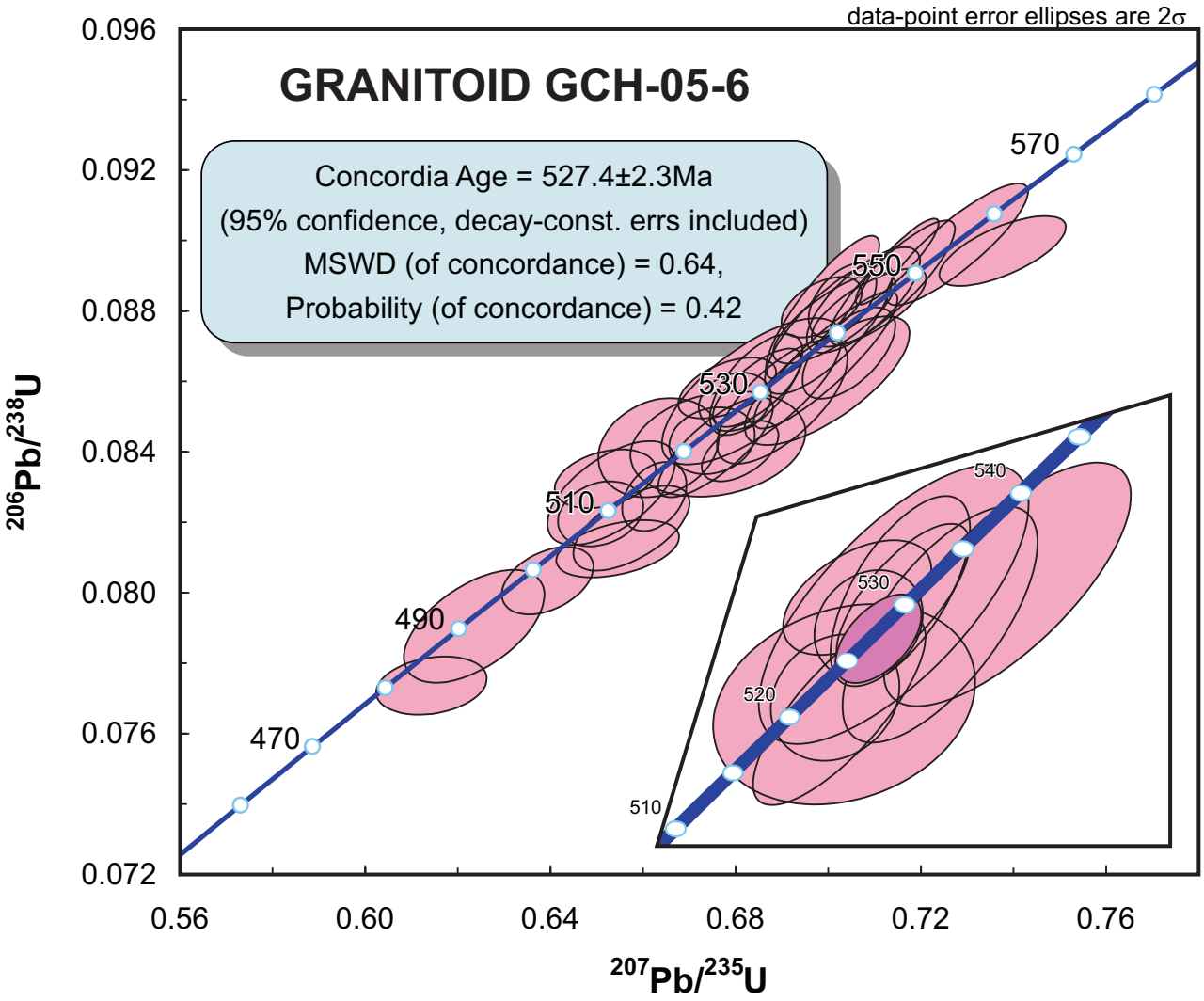

Fig. 9.- U-Pb concordia diagram showing the results of LA-ICP-MS zircon analyses from metagranitoid GCH-05-6. The enlarged region shows a concordia age calculated from 10 concordant and overlapping analyses. Error ellipses are ± 2σ.

Fig. 9.- Diagrama de concordia U-Pb con la proyección de los circones analizados mediante LA-ICP-MS en el metagranitoide GCH-05-6. La región ampliada muestra una edad de concordia calculada a partir de 10 análisis concordantes y superpuestos. Las elipses de error son ± 2σ.

considering the statistical uncertainty of a single analysis, we favour a lower to middle Ordovician time interval for the sedimentation as the zircon population increases dramatically during this period (Fig. 10b). Zircons in the age range of 500-750 Ma which constitute the main population in this sample (Fig. 10), correspond to the Cadomian-Avalonian-Pan-African events (Fernandez-Suárez *et al.*, 2002; Linnemann *et al.*, 2004) and they are lacking in sediments with a provenance from the Baltica craton. The presence of a population with Palaeoproterozoic ages in the interval of c. 1800-2200 Ma (Fig. 10), together with the absence of the Mesoproterozoic population between 900-1100 Ma, which appears in sediments derived from the Amazonia Craton (Nance and Murphy, 1994), is typical of a West-African provenance (Eburnian events). On the other hand, the population of Archaean ages (Fig. 10b) can be related to Liberian events from Africa (Fernandez-Suárez *et al.*, 2002). In conclusion, these age populations indicate that the deposition of these conglomerates was adjacent to the Gondwana margin.

5. Geochemistry of the igneous rocks

A set of 27 samples of the most representative igneous rocks from the Somozas Mélange were collected in order to study their geochemical composition. These rocks are typical members of the ophiolitic mélange, and they include: 13 samples corresponding to different types of metavolcanic rocks, some of them clearly submarine, 6 diabase dikes and 8 different types of gabbros, diorites and granitoids. The milling of these samples was performed at the Universidad Complutense de Madrid and

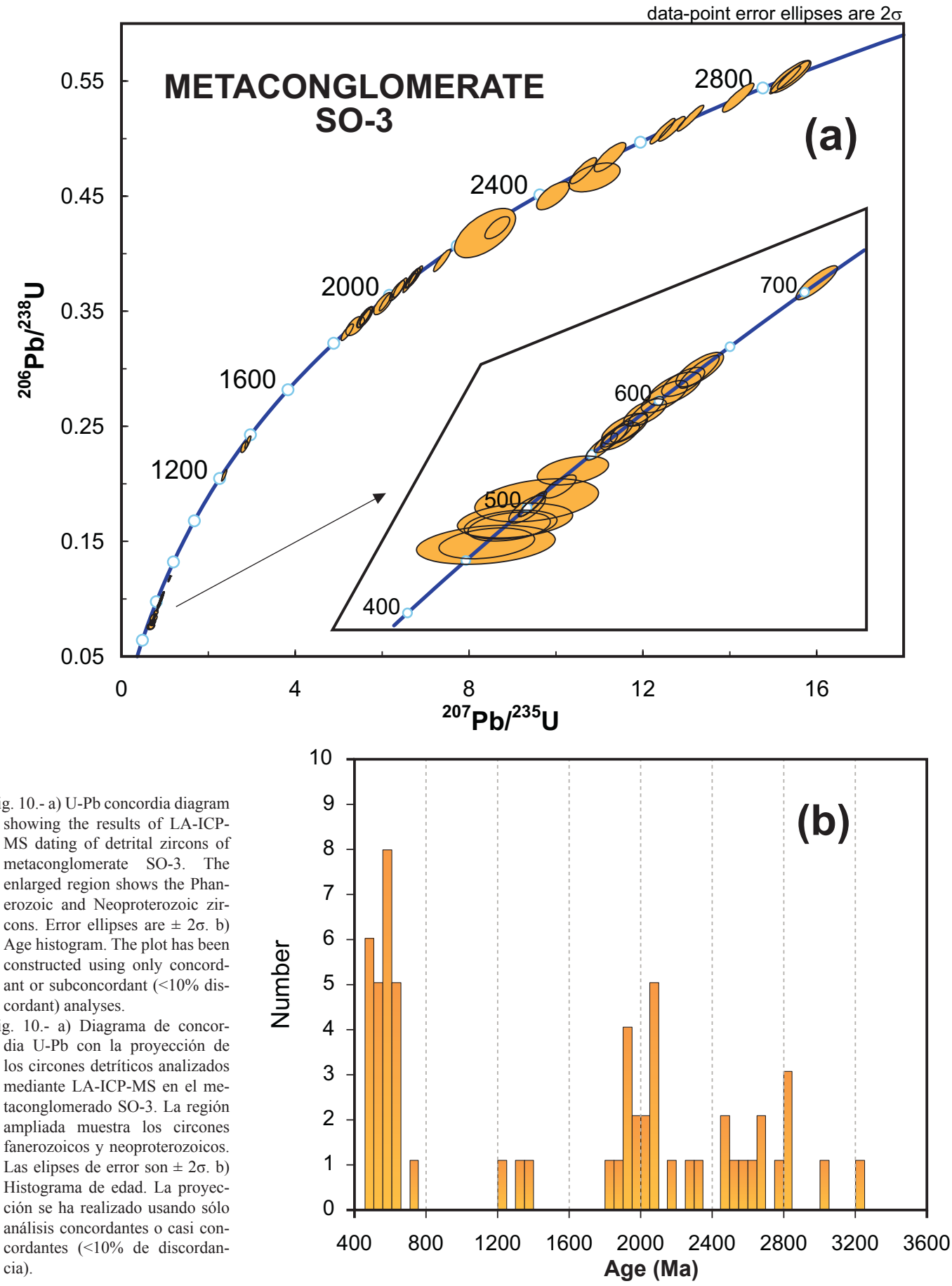

Fig. 10.- a) U-Pb concordia diagram showing the results of LA-ICP-MS dating of detrital zircons of metaconglomerate SO-3. The enlarged region shows the Phanerozoic and Neoproterozoic zircons. Error ellipses are ± 2σ. b) Age histogram. The plot has been constructed using only concordant or subconcordant (<10% discordant) analyses.

Fig. 10.- a) Diagrama de concordia U-Pb con la proyección de los circones detríticos analizados mediante LA-ICP-MS en el metaconglomerado SO-3. La región ampliada muestra los circones fanerozoicos y neoproterozoicos. Las elipses de error son ± 2σ. b) Histograma de edad. La proyección se ha realizado usando sólo análisis concordantes o casi concordantes (<10% de discordancia).

they were analysed at the Activation Laboratories Ltd. (Actlabs) in Canada. The digestion procedure was the lithium metaborate/tetraborate fusion, and the analytical technique used to measure the elemental concentrations was inductively coupled plasma mass spectrometry (ICP-MS). The results obtained appear in Tables 5 to 8.

5.1. General geochemical features and classification

Two main groups of metavolcanic rocks can be distinguished in the Somozas Mélange, submarine volcanic rocks whose most representative outcrops are located in the Espasante locality, in the coast section (Fig. 3), and common metavolcanic rocks. The 6 samples corresponding to the first group are characterized by SiO_2 contents ranging between 49.75 and 51.88 that allow their classification as basic rocks. The compositional ranges of the rest of the major elements for them vary: 17.84-18.92% Al_2O_3, 8.46-9.57% Fe_2O_3(T), 0.15-0.29% MnO, 3.94-4.7% MgO, 8.92-9.84% CaO, 2.04-2.76% Na_2O, 0.11-0.34% K_2O, 0.99-1.01% TiO_2, and 0.15-0.18% P_2O_5 (Table 5). The samples of common metavolcanics are also metabasites with slightly lower SiO_2 contents (48.06-51.64%). Regarding the rest of the major elements, their composition is lower in Al_2O_3, CaO, K_2O, TiO_2, P_2O_5 (14.34-15.81%, 5.84-9.6%, 0.02-0.22%, 0.69-0.94%, 0.04-0.09%, respectively) and higher in Fe_2O_3(T), MgO and Na_2O (9.92-11.52%, 7.3-9.66%, 2.7-4.48%, respectively) compared to that of the submarine volcanic rocks (Table 6).

The diabase dikes appear in the same outcrops of Espasante where the analyzed submarine volcanic rocks were taken. These dikes show clear intrusive relationships with all the submarine volcanic rocks, including the lava flows, the submarine breccias and the pillow lavas. The compositional range of the diabase dikes is very narrow and they have compositions of mafic rocks (48.93-49.24% SiO_2) with contents in major elements ranging: 15.06-15.58% Al_2O_3, 11.76-12.41% Fe_2O_3(T), 0.22-0.23% MnO, 6.16-6.49% MgO, 9.42-10.6% CaO, 0.24-0.58% Na_2O, 0.01-0.08% K_2O, 1.57-1.63% TiO_2, and 0.12-0.16% P_2O_5 (Table 7).

One of the plutonic rocks has a SiO_2 content typical of mafic rocks (sample CE-99, 51.78%), three have intermediate compositions (samples CE-92, CE- 93 and CE-95; 53.61-54.43% SiO_2), and the rest are felsic granitoids with SiO_2 content ranging between 69.76-72.58%. The metabasite sample can also be distinguished from the samples of intermediate composition according to its lower contents in CaO and K_2O, and higher Fe_2O_3(T), MnO, Na_2O, TiO_2 and P_2O_5 (Table 8).

Secondary processes such as hydrothermal alteration, metamorphism or deformation may have alterated the primary compositions of the rocks. Therefore, the chemical classification of the mélange samples uses a combination of diagrams based in mobile (silica and alkalis, Fig. 11a) and immobile (Ti, Zr, Nb and Y, Fig. 11b) elements. According to them, all the investigated samples of the Somozas Mélange have compositions typical of subalkaline rocks. It is possible to chemically distinguish quite clearly the two different types of metavolcanic rocks, given that the Espasante submarine metavolcanics can be classified as basaltic andesites whereas the common metavolcanic rocks are more similar to basalts. This difference is more marked in their immobile trace element contents. Same differences exist between the mafic and the intermediate plutonic rocks; a sample of gabbro has compositions equivalent to a basalt and the intermediate rocks have compositions compatible with basaltic andesites. The felsic granitoids have compositions equivalent to that of rhyodacites.

The submarine metavolcanics have total rare earth element (∑REE) contents ranging between 75 and 81 ppm, and concentrations between 9 and 40 times the chondritic abundances (Nakamura, 1974). They show fractionated chondrite-normalized REE patterns ($[La/Yb]_N$ = 3.63-3.84, Fig. 12a) typical of calc-alkaline rocks, enriched in light REE (LREE) compared to the heavy REE (HREE), with slightly negative Eu anomalies (Eu/Eu* = 0.86-0.89; calculated according to Taylor and MacLennan, 1985). The common metavolcanics have very lower ∑REE, ranging between 20 and 30 ppm and concentrations between 3 and 12 times the chondritic abundances. Their chondrite-normalized REE patterns (Fig. 12b) are parallel although depleted compared to that corresponding to a typical N-MORB according to Pearce and Parkinson (1993). These are almost flat for the HREE ($[Gd/Yb]_N$ = 0.82-1.05) and depleted on LREE compared to the HREE ($[La/Sm]_N$ = 0.43-0.70), without significant Eu anomalies (Eu/Eu* = 0.88-1.14). The samples of diabase dikes have total REE contents ranging between 55 and 71 ppm, and concentrations between 12 and 30 times the chondritic abundances. They show relatively flat normalized REE patterns, although slightly enriched in LREE relative to HREE ($[La/Yb]_N$ = 1.19-1.78, Fig. 12c), and without significant Eu anomalies (Eu/Eu* = 0.88-1.14). The gabbroic sample has total REE contents in the same range than the common volcanics (27 ppm). It shows concentrations between 4 and 11 times the chondritic abundances and its normalized REE pattern (Fig. 12d) is almost flat for the HREE ($[Gd/Yb]_N$ = 0.87) and depleted in light LREE compared to the HREE ($[La/Sm]_N$ = 0.51),

TABLE 5.- WHOLE ROCK MAJOR AND TRACE ELEMENT DATA OF ESPASANTE SUBMARINE VOLCANIC ROCKS.

Sample	CI-7	CI-8	CI-9	CI-10	CI-11	CI-12
SiO_2	50.53	49.75	51.33	51.69	51.88	51.42
Al_2O_3	18.54	18.92	18.46	18.28	18.3	17.84
Fe_2O_3	9.08	9.57	8.84	8.71	8.61	8.46
MnO	0.165	0.289	0.151	0.158	0.155	0.203
MgO	4.27	4.7	4.12	3.94	4.03	4.54
CaO	9.34	9.23	9.19	9.84	8.92	9.22
Na_2O	2.76	2.04	2.33	2.28	2.53	2.35
K_2O	0.34	0.11	0.26	0.17	0.34	0.2
TiO_2	1.006	0.992	1.003	0.998	0.992	0.995
P_2O_5	0.15	0.17	0.17	0.17	0.16	0.18
LOI[1]	3.24	3.72	3.34	3.12	3.17	3.41
TOTAL	99.42	99.49	99.19	99.36	99.09	98.82
Sc	28	29	27	27	28	28
V	189	187	186	197	182	201
Cr	40	70	60	70	70	50
Co	17	20	20	19	19	19
Ni	< 20	20	20	50	20	< 20
Cu	40	110	50	30	40	50
Zn	< 30	120	80	80	80	120
Ga	17	19	18	17	17	17
Rb	8	3	5	5	11	5
Sr	296	327	314	333	314	307
Y	27	26.9	26.4	24.1	24.8	24.2
Zr	93	100	101	95	104	98
Nb	3.1	3.1	3.3	3	3.2	3
Cs	0.4	0.3	0.4	0.3	0.8	0.4
Ba	211	87	179	181	197	182
Hf	2.8	2.8	2.7	2.6	2.9	2.7
Ta	0.19	0.19	0.2	0.18	0.2	0.18
Pb	< 5	7	< 5	7	5	9
Th	3.02	3.06	3.06	3.03	3.08	2.86
U	1.28	1.29	1.28	1.31	1.37	1.28
La	12.8	13	12.3	12.7	12.3	11.8
Ce	27.3	27.7	25.8	27	26.6	25.9
Pr	3.73	3.75	3.52	3.62	3.55	3.41
Nd	16.1	15.9	15.9	16	15.4	15.4
Sm	4.09	3.82	3.8	3.71	3.8	3.61
Eu	1.19	1.14	1.08	1.1	1.13	1.08
Gd	4.11	4.16	3.89	3.98	4.04	3.86
Tb	0.71	0.69	0.7	0.68	0.66	0.64
Dy	4.33	4.24	4.08	3.97	3.92	3.84
Ho	0.89	0.87	0.83	0.78	0.78	0.75
Er	2.65	2.6	2.47	2.36	2.4	2.26
Tm	0.383	0.38	0.362	0.358	0.352	0.336
Yb	2.36	2.34	2.25	2.21	2.22	2.13
Lu	0.34	0.339	0.322	0.31	0.311	0.291
Σ REE	80.98	80.93	77.30	78.78	77.46	75.31
Eu/Eu*	0.89	0.88	0.86	0.88	0.89	0.89
$(La/Sm)_N$	1.93	2.10	2.00	2.11	2.00	2.02
$(Gd/Yb)_N$	1.39	1.42	1.38	1.44	1.45	1.44
$(La/Yb)_N$	3.63	3.71	3.66	3.84	3.70	3.70

[1]Loss on ignition.
Oxides are in weight percent (%). Trace and rare earth elements are in parts per million (ppm).
The element concentrations expressed with the < sign are below detection limit.

Table 5. Whole rock major and trace element data of the Espasante submarine volcanic rocks.
Tabla 5. Análisis químicos de elementos mayores y traza de las rocas volcánicas submarinas de Espasante.

TABLE 6.- WHOLE ROCK MAJOR AND TRACE ELEMENT DATA OF COMMON VOLCANIC ROCKS.

Sample	CE-100	CE-101	CE-102	CE-103	CE-104	CE-105	CE-107
SiO_2	50.17	49.5	48.92	48.06	51.64	49.1	49.07
Al_2O_3	15.03	14.97	14.34	15.38	15.28	15.81	14.78
Fe_2O_3	11.52	10.5	10.64	11.11	10.83	10.43	9.92
MnO	0.179	0.143	0.15	0.154	0.198	0.185	0.171
MgO	8.24	8.38	9.4	8.51	7.67	7.3	9.66
CaO	5.84	7.8	8.22	9.36	6.04	9.6	8.85
Na_2O	2.7	3.96	3.36	2.74	4.48	3.17	3.09
K_2O	0.02	0.04	0.22	0.05	0.1	0.09	0.12
TiO_2	0.936	0.91	0.885	0.885	0.706	0.748	0.691
P_2O_5	0.07	0.08	0.08	0.09	0.05	0.06	0.04
LOI[1]	4.77	2.81	2.94	3.21	2.86	2.73	3.19
TOTAL	99.47	99.09	99.16	99.55	99.85	99.22	99.58
Sc	40	40	38	42	43	44	46
V	288	279	271	273	270	281	248
Cr	260	280	330	320	100	170	430
Co	35	37	39	34	37	36	36
Ni	50	90	110	80	30	40	100
Cu	110	50	50	70	90	70	70
Zn	140	50	60	70	60	40	50
Ga	16	15	16	14	12	14	12
Rb	< 1	< 1	3	< 1	< 1	1	2
Sr	62	90	73	107	32	23	109
Y	21.1	20.1	21.2	23.3	18.2	20	19
Zr	41	40	40	43	30	30	25
Nb	0.6	0.5	0.5	0.5	0.3	0.3	0.3
Cs	0.3	0.1	0.4	0.1	< 0.1	< 0.1	0.1
Ba	8	16	29	11	16	22	29
Hf	1.4	1.3	1.2	1.4	1	1	0.8
Ta	0.02	0.02	0.02	0.01	< 0.01	< 0.01	< 0.01
Pb	< 5	< 5	< 5	< 5	< 5	< 5	< 5
Th	0.2	0.19	0.17	0.24	0.12	0.14	0.07
U	0.12	0.12	0.12	0.19	0.15	0.17	0.06
La	1.81	1.74	1.81	2	0.86	1.18	1.65
Ce	5.21	5.03	5.1	5.36	2.78	3.42	3.32
Pr	0.92	0.9	0.92	0.99	0.53	0.62	0.67
Nd	5.25	5.06	5.37	5.57	3.32	3.82	4.22
Sm	1.79	1.75	1.84	1.95	1.23	1.45	1.46
Eu	0.73	0.743	0.83	0.768	0.476	0.526	0.57
Gd	2.72	2.65	2.71	3.08	1.99	2.34	2.13
Tb	0.53	0.51	0.51	0.59	0.41	0.49	0.43
Dy	3.37	3.28	3.33	3.73	2.85	3.22	2.93
Ho	0.72	0.69	0.71	0.8	0.63	0.7	0.63
Er	2.19	2.06	2.25	2.49	1.95	2.15	1.87
Tm	0.328	0.306	0.344	0.372	0.294	0.328	0.272
Yb	2.15	2.02	2.18	2.39	1.93	2.17	1.73
Lu	0.32	0.299	0.317	0.373	0.308	0.33	0.267
Σ REE	28.04	27.04	28.22	30.46	19.56	22.74	22.15
Eu/Eu*	1.02	1.06	1.14	0.96	0.94	0.88	0.99
$(La/Sm)_N$	0.62	0.61	0.61	0.63	0.43	0.50	0.70
$(Gd/Yb)_N$	1.01	1.05	0.99	1.03	0.82	0.86	0.98
$(La/Yb)_N$	0.56	0.58	0.56	0.56	0.30	0.36	0.64

[1]Loss on ignition.

Oxides are in weight percent (%). Trace and rare earth elements are in parts per million (ppm).

The element concentrations expressed with the < sign are below detection limit.

Table 6. Whole rock major and trace element data of common volcanic rocks.

Tabla. 6. Análisis químicos de elementos mayores y traza de las rocas volcánicas comunes.

TABLE 7.- WHOLE ROCK MAJOR AND TRACE ELEMENT DATA OF ESPASANTE DYKES

Sample	CI-1	CI-2	CI-3	CI-4	CI-5	CI-6
SiO_2	49.06	49.15	49.07	48.96	48.93	49.24
Al_2O_3	15.21	15.39	15.24	15.27	15.06	15.58
Fe_2O_3	12.41	12.1	12.17	12.27	12.15	11.76
MnO	0.224	0.228	0.223	0.216	0.225	0.231
MgO	6.31	6.37	6.39	6.25	6.49	6.16
CaO	9.58	9.68	9.5	9.42	9.82	10.6
Na_2O	0.36	0.32	0.45	0.58	0.29	0.24
K_2O	0.03	0.08	< 0.01	0.02	0.02	< 0.01
TiO_2	1.613	1.598	1.63	1.634	1.628	1.566
P_2O_5	0.12	0.15	0.16	0.16	0.15	0.15
LOI[1]	4.18	3.95	4.21	4.42	4.01	3.99
TOTAL	99.1	99.02	99.04	99.2	98.77	99.52
Sc	39	39	40	40	40	38
V	295	294	300	297	302	287
Cr	110	90	100	110	100	150
Co	24	33	31	31	32	31
Ni	40	50	50	50	50	80
Cu	50	30	60	50	50	40
Zn	50	130	90	90	120	90
Ga	17	18	18	17	18	18
Rb	< 1	< 1	< 1	< 1	< 1	< 1
Sr	240	280	231	236	286	299
Y	35.1	32.9	33.4	32.8	40.8	32.1
Zr	88	89	90	90	91	87
Nb	1.7	1.6	1.7	1.6	1.7	1.8
Cs	0.1	0.1	0.2	0.2	< 0.1	0.1
Ba	29	15	30	20	22	20
Hf	2.6	2.5	2.7	2.5	2.6	2.5
Ta	0.09	0.08	0.09	0.08	0.08	0.07
Pb	< 5	8	< 5	7	7	6
Th	0.6	0.56	0.61	0.58	0.59	0.54
U	0.24	0.36	0.24	0.24	0.25	0.22
La	5.95	5.89	5.7	5.64	10	5.3
Ce	14	13.8	14.1	13.7	14.1	13.5
Pr	2.29	2.25	2.24	2.17	2.93	2.11
Nd	11.4	11.4	11.2	11.2	14.2	10.8
Sm	3.73	3.62	3.61	3.47	4.25	3.37
Eu	1.42	1.4	1.4	1.37	1.63	1.33
Gd	4.75	4.55	4.6	4.6	5.56	4.25
Tb	0.87	0.85	0.85	0.82	1.04	0.79
Dy	5.5	5.37	5.38	5.36	6.67	4.99
Ho	1.15	1.11	1.11	1.13	1.39	1.04
Er	3.35	3.32	3.28	3.28	4.17	3.21
Tm	0.502	0.482	0.48	0.476	0.611	0.473
Yb	3.25	2.98	3.05	2.92	3.78	2.99
Lu	0.468	0.425	0.438	0.428	0.531	0.418
Σ REE	58.63	57.45	57.44	56.56	70.86	54.57
Eu/Eu*	1.04	1.06	1.06	1.05	1.03	1.08
$(La/Sm)_N$	0.98	1.00	0.97	1.00	1.45	0.97
$(Gd/Yb)_N$	1.16	1.22	1.20	1.26	1.17	1.13
$(La/Yb)_N$	1.22	1.32	1.25	1.29	1.77	1.19

[1]Loss on ignition.
Oxides are in weight percent (%). Trace and rare earth elements are in parts per million (ppm).
The element concentrations expressed with the < sign are below detection limit.

Table 7. Whole rock major and trace element data of the Espasante dikes.
Tabla 7. Análisis químicos de elementos mayores y traza de los diques de Espasante.

TABLE 8.- WHOLE ROCK MAJOR AND TRACE ELEMENT DATA OF GABBROIC ROCKS AND GRANITOIDS

Sample	CE-92	CE-93	CE-95	CE-99	CE-94	CE-96	CE-97	CE-98
SiO_2	54.43	53.96	53.61	51.78	69.76	72.58	71.44	70.4
Al_2O_3	16.67	15.29	17.36	15.28	14.29	13.84	13.84	14.04
Fe_2O_3	7.42	7.3	6.37	11.02	3.68	3	2.44	2.66
MnO	0.105	0.126	0.113	0.203	0.042	0.034	0.032	0.047
MgO	7.07	8.77	6.57	7.28	2.01	1.34	1.4	2.06
CaO	7.23	5.86	6.93	4.7	0.67	1.43	0.53	0.58
Na_2O	2.97	3.25	2.44	4.79	6.44	6.15	2.74	3.38
K_2O	0.94	1.57	2.68	0.07	0.51	0.35	4.28	3.55
TiO_2	0.336	0.271	0.256	0.896	0.361	0.355	0.473	0.5
P_2O_5	0.04	0.04	0.04	0.06	0.08	0.09	0.14	0.15
LOI[1]	2.54	2.92	2.89	3.25	1.28	0.87	1.71	1.8
TOTAL	99.75	99.36	99.26	99.33	99.12	100.04	99.03	99.17
Sc	27	29	31	43	11	7	10	9
V	176	177	261	312	50	40	18	16
Cr	140	160	130	60	140	90	120	100
Co	17	23	21	40	7	5	2	3
Ni	80	120	40	< 20	< 20	< 20	< 20	< 20
Cu	20	50	< 10	60	30	30	< 10	< 10
Zn	< 30	30	40	50	< 30	< 30	< 30	40
Ga	13	12	17	17	13	14	17	18
Rb	24	48	91	1	13	8	129	110
Sr	266	105	104	84	101	137	78	62
Y	11.2	11.2	10.4	22.9	18.7	18	43.4	45.3
Zr	33	34	37	37	89	87	146	163
Nb	1.1	1	1.8	0.8	3.6	3.5	12.2	12.6
Cs	0.7	1.5	2.8	< 0.1	0.4	0.6	2.3	3.2
Ba	164	268	378	13	180	131	938	729
Hf	1.1	1	1	1.3	2.4	2.5	4	4.5
Ta	0.06	0.06	0.13	0.01	0.33	0.33	1.05	1.03
Pb	< 5	< 5	< 5	< 5	< 5	< 5	< 5	25
Th	1.15	1.45	1.68	0.31	4.31	4.23	14.5	15.9
U	0.63	0.74	0.96	0.18	2.4	2.48	7.25	4.26
La	4.39	4.72	5.88	1.44	12	12.4	40.9	44.2
Ce	8.57	8.97	11.8	4.28	24.2	23.1	76.1	88.5
Pr	1.14	1.17	1.48	0.78	2.87	2.79	9.35	10.5
Nd	4.66	4.59	5.83	4.61	11	10.3	34.5	39.7
Sm	1.25	1.24	1.34	1.73	2.36	2.26	6.94	7.97
Eu	0.428	0.438	0.51	0.676	0.734	0.606	1.28	1.46
Gd	1.49	1.45	1.51	2.74	2.64	2.56	6.86	8.04
Tb	0.27	0.26	0.26	0.55	0.47	0.45	1.14	1.3
Dy	1.71	1.74	1.64	3.68	2.8	2.71	6.52	7.48
Ho	0.37	0.37	0.34	0.79	0.59	0.57	1.32	1.45
Er	1.14	1.12	1.04	2.46	1.84	1.77	4.1	4.24
Tm	0.173	0.176	0.158	0.386	0.287	0.283	0.61	0.629
Yb	1.09	1.13	1.06	2.52	1.91	1.83	3.72	3.96
Lu	0.165	0.169	0.163	0.389	0.292	0.277	0.536	0.563
Σ REE	26.85	27.54	33.01	27.03	63.99	61.91	193.88	219.99
Eu/Eu*	0.96	1.00	1.10	0.95	0.90	0.77	0.57	0.56
$(La/Sm)_N$	2.17	2.35	2.71	0.51	3.14	3.39	3.64	3.42
$(Gd/Yb)_N$	1.09	1.02	1.14	0.87	1.10	1.12	1.47	1.62
$(La/Yb)_N$	2.69	2.79	3.71	0.38	4.20	4.53	7.35	7.46

Samples CE-92, CE-93 and CE-95 are gabbros type I, sample CE-99 is a gabbro type II, and samples CE-94, CE-96, CE-97 and CE-98 are granitoids.
[1]Loss on ignition.
Oxides are in weight percent (%). Trace and rare earth elements are in parts per million (ppm).
The element concentrations expressed with the < sign are below detection limit.

Table 8. Whole rock major and trace element data of gabbroic rocks and granitoids.

Tabla 8. Análisis químicos de elementos mayores y traza de las rocas gabroicas y granitoides.

without a significant Eu anomaly (Eu/Eu* = 0.95), very similar to those of the common metavolcanics. The intermediate plutonic rock samples, although having similar total REE to the gabbroic sample (27-33 ppm, from 4 to 18 times the chondritic abundances), have fractionated REE patterns an enrichment of the LREE compared to the HREE ($[La/Yb]_N$ = 2.69-3.71, Fig. 12d) and without significant Eu anomalies (Eu/Eu* = 0.96-1.10). These are comparable to submarine volcanics, although they are more depleted, suggesting they are less evolved lithologies. Regarding the granitoids, it is possible to distinguish two of them with low REE contents (62-64 ppm, from 7 to 38 times the chondritic abundances) and the other two more enriched (194-220 ppm, from 16 to 134 times the chondritic abundances), that are also the most evolved according to their higher Ti/Nb and Zr/Y ratios. All of them have fractionated chondrite-normalized REE patterns that are steeper in the case of the most enriched samples ($[La/Yb]_N$ = 4.20-4.53, in samples CE-94 and CE-96, and 7.35-7.46 in samples CE-97 and CE-98; Fig. 12e), with a significant negative Eu anomaly, most marked in the REE-enriched samples.

5.2. Tectonic setting

The most useful geochemical discrimination diagrams to determine the tectonic setting of the Somozas Mélange rocks are Ti-Zr-Y (Pearce and Cann, 1973), Th-Hf-Ta (Wood, 1980), MnO-TiO_2-P_2O_5 (modified after Mullen, 1983), Ta/Yb-Th/Yb (Pearce, 1983) and Ta-Yb (Pearce *et al.*, 1984), which are essentially based on immobile trace and major elements. The last two diagrams are suitable for felsic rocks, specially the Ta-Yb diagram that was specifically designed to identify granitoid types. In the Ti-Zr-Y, the mélange samples plot forming two distinguished groups; the first, including the common volcanics, dikes and the gabbro sample is located in or near the field of island-arc tholeiites, and the second group, consisting in the submarine metavolcanics and the intermediate plutonic rocks, is located in the calc-alkali basalts field (Fig. 13a). The Th-Hf-Ta diagram allows the most accurate discrimination of subduction related rocks. All the samples collected from the Somozas Mélange plot in the field corresponding to rocks generated in destructive plate margins (Fig. 13b), due to their low Ta contents. It is possible to distinguish between samples with tholeiitic affinity (common metavolcanics, dikes and gabbro) which have Hf/Th $\geq$ 4.2, and samples with calc-alkaline affinity (submarine metavolcanics, intermediate plutonic rocks and acid granitoids) characterized by Hf/Th $\leq$ 0.96. Their projection in the MnO-TiO_2-P_2O_5 diagram confirms this origin for the mafic and intermediate samples of the Somozas Mélange as they are located near the apex corresponding to supra-subduction zone rocks (Fig. 13c). All the mafic and intermediate samples with Ta/Yb ratios higher than 0.01 plot in the subduction-related field of the Ta/Yb-Th/Yb diagram far from the mantle array (Fig. 13d). All of them show Th/Yb ratios higher than typical N-MORB, but compatible with that of island-arc tholeiites in the case of the diabase dikes (Th/Yb = 0.156-0.2). The ratios of the common volcanics and the intermediate plutonic rocks are even higher (Th/Yb = 1.055-1.585), indicating calc-alkaline affinity, and their Ta/Yb ratios are intermediate between those typical of rocks generated in oceanic arcs and active continental margins (Ta/Yb = 0.053-0.123). The Ta-Yb diagram confirms the origin in a supra-subduction zone for the Somozas Mélange acid granitoids, showing that their compositions are similar to that of volcanic arc granites (Fig. 14e).

Trace element abundance diagrams normalized to the average composition of rocks of a typical dynamic origin have been plotted for each group of samples to determine more accurately their tectonic setting. The average N-MORB composition (Pearce, 1996) has been the normalizing factor used to plot all the mélange samples, except for the felsic granitoids, which were normalized to the ORG composition (Pearce *et al.*, 1984). Both the compositional range of each lithological type and their average composition are represented in Figure 14. As can be observed, a quite clear resemblance exists between the patterns corresponding to the samples of submarine metavolcanics and the intermediate plutonic rocks, and between those corresponding to the common metavolcanics, dikes and gabbro. The two first lithological types are characterized by strongly fractionated trace element patterns (Fig 14a, d and e) with a marked Nb anomaly, although the intermediate plutonic rocks are more depleted in all the elements, suggesting that they are less evolved lithologies. Both submarine volcanics and intermediate rocks are strongly enriched in Th compared to N-MORB. The metavolcanics are also enriched in Ce, slightly depleted in Ti, but with similar concentrations in Nb, Zr and Y compared to the typical N-MORB composition (Fig. 14a and e). The intermediate rocks are depleted in Nb, Zr, Ti and Y compared to the N-MORB and have similar Ce contents (Fig. 14d and e). The significant Nb anomaly present in all the samples clearly indicates an origin in a subduction zone environment, whereas the strong fractionation of their trace element patterns is typical of calc-alkalic rocks, which suggest that they were probably generated in an evolved volcanic arc. Common volcanics, diabase dikes and gabbro are characterized by trace

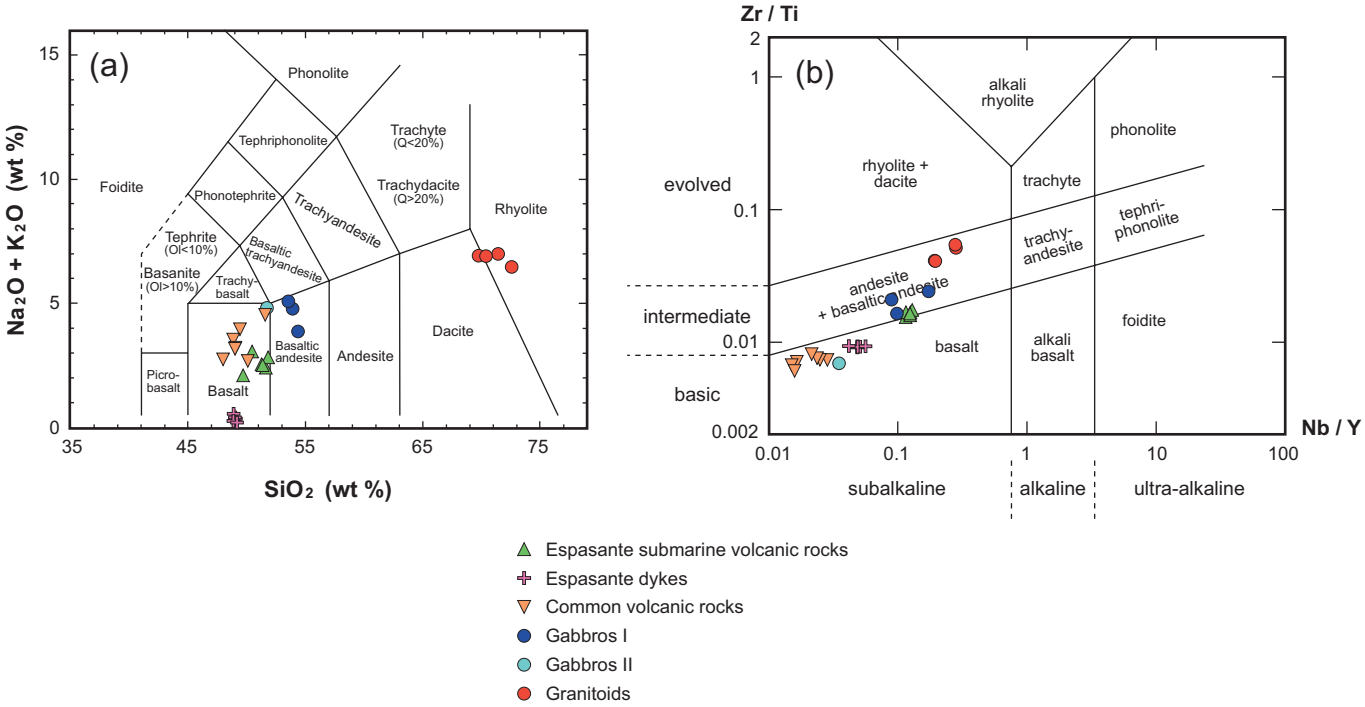

Fig. 11.- a) Total alkalis vs. SiO_2 diagram (Le Maitre *et al.*, 1989). b) Zr/Ti – Nb/Y diagram of Winchester and Floyd (1977), modified by Pearce (1996); Ol, olivine; Q, quartz.

Fig. 11.- a) Diagrama álcalis totales vs. SiO_2 (Le Maitre *et al.*, 1989). b) Diagrama Zr/Ti - Nb/Y de Winchester and Floyd (1977), modificado por Pearce (1996); Ol, olivino; Q, cuarzo.

element patterns essentially parallel to that of N-MORB, except for their marked Nb anomaly (Fig. 14b, c and e). The common metavolcanics are the most depleted samples, with lower contents in Nb, Ce Zr, Ti and Y than those of the average N-MORB (Fig. 14b and e). The diabase dikes have higher contents in trace elements than the common metavolcanics. In relation to N-MORB they show similar abundance of Zr, Ti and Y, but they are enriched in Th and Ce and depleted in Nb (Fig. 14c and e). The gabbro has a trace element pattern very similar to that of the common metavolcanics (Fig. 14d and e), although slightly enriched in Th and Nb than these samples. The geochemical features of these three lithologics, such as their trace element contents similar to N-MORB, together with their little fractionated patterns indicate their tholeiitic affinity, whereas their marked Nb anomaly suggests a subduction-related origin. The granitoids are characterized by strongly fractionated trace element patterns and generally depleted trace element abundances compared to ORG, except for the strong enrichment in Th, and some samples with slight enrichment in Ce. The most significant feature of their patterns is a pronounced negative Ta and Nb anomaly, which together with their low contents in Y and Yb are typical of granitoids generated in volcanic arcs or subduction zones.

In summary, according to the information provided by the trace elements with the most immobile behaviour and the highest discriminating power, submarine metavolcanics, intermediate plutonic rocks and granitoids of the Somozas Mélange are classified as calc-alkaline rocks which were generated in a supra-subduction zone setting, probably during the mature stages of the evolution of a volcanic arc. However, common metavolcanics, diabase dikes and gabbro show geochemical features compatible with that of island arc tholeiites, also related to the activity of a subduction zone.

6. The origin of the Somozas Mélange

6.1. Interpretation of the U-Pb and geochemical data

Whole rock geochemical data show that two igneous series with different composition are represented in the Somozas Mélange. Both suites contain plutonic and volcanic members: an igneous series with calc-alkaline composition and another one equivalent to island-arc tholeiites. It is difficult to clarify the relative chronology of both series and their possible regional coexistence, as they are restricted to the tectonic blocks and slices involved in the mélange. However, there are key exposures

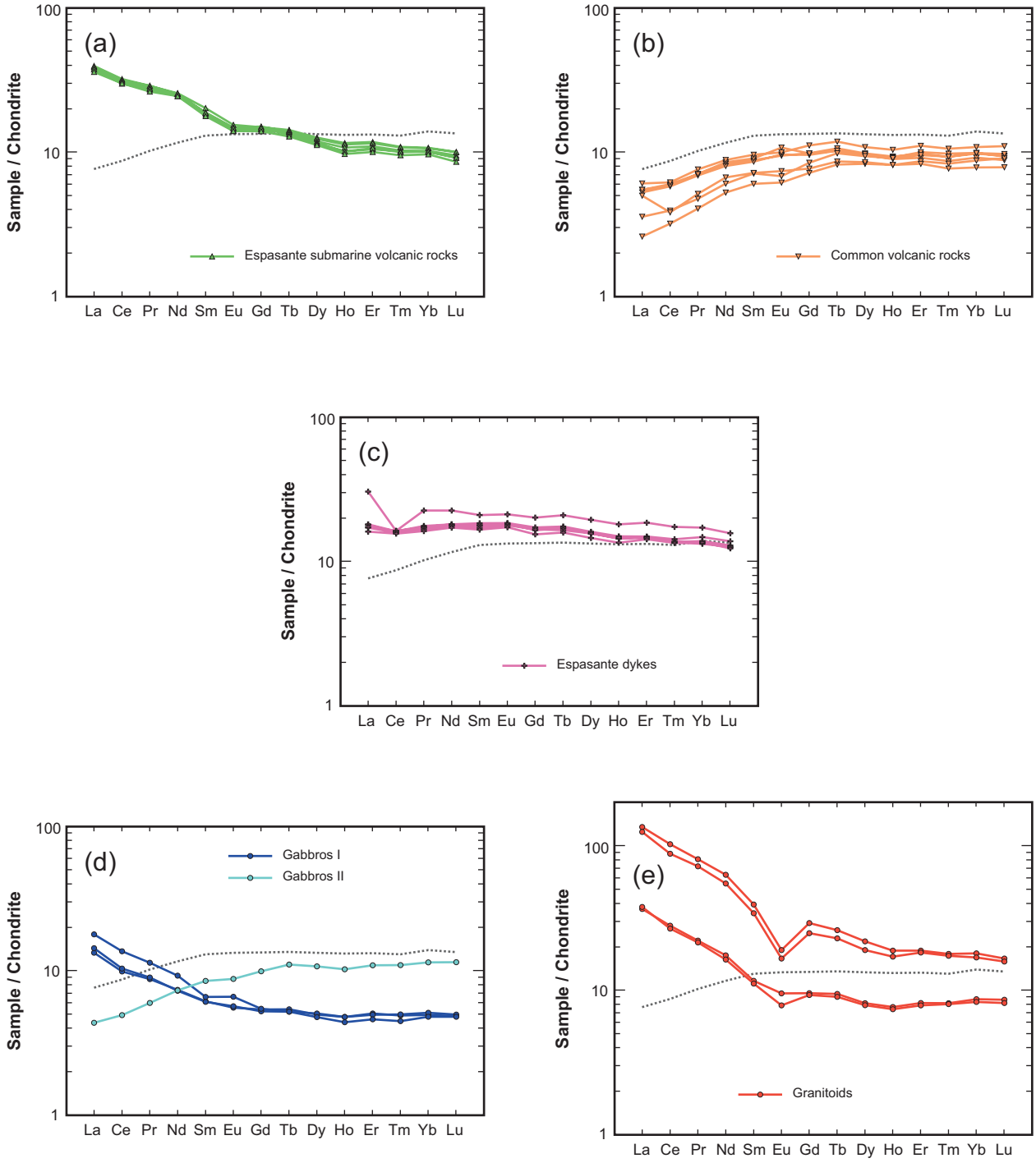

Fig. 12.- Chondrite-normalized rare earth elements plots for the igneous rocks distinguished in the Somozas Mélange; normalizing values are from Nakamura (1974). The dotted line corresponds to a typical N-MORB according to Pearce and Parkinson (1993).

Fig. 12.- Proyecciones de las tierras raras normalizadas a la condrita, para los grupos ígneos distinguidos en la Mélange de Somozas; los valores de normalización son los de Nakamura (1974). La línea de puntos corresponde a un N-MORB típico, según Pearce and Parkinson (1993).

in the coastal section, around the Espasante village (Fig. 3), suggesting that both series shared a common paleogeographic origin, but they were probably formed at different times. These outcrops define a thick tectonic slice constituted by calc-alkaline volcanic rocks with broken pillow breccias, close-packed pillow lavas and lava flows, intruded by a set of diabase dikes with compositions of island-arc tholeiites (Arenas and Peinado, 1981; Arenas, 1985). Moreover calc-alkaline rocks, either mafic or felsic, which are rather common in the ophiolitic

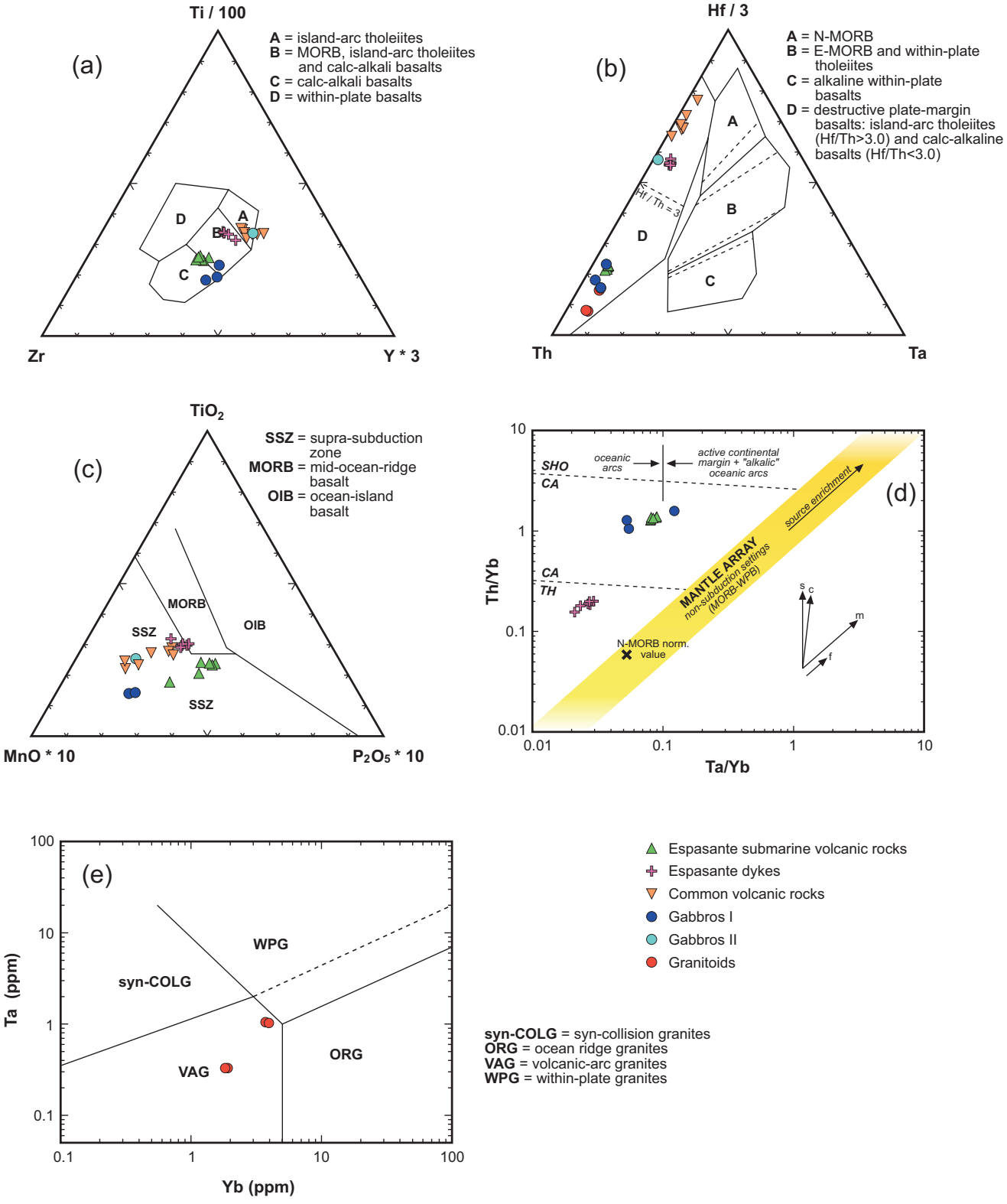

Fig. 13.- Trace elements tectonic discrimination diagrams for the samples of the Somozas Mélange. a) Ti-Zr-Y diagram (Pearce and Cann, 1973). b) Hf-Th-Ta diagram (Wood, 1980). c) TiO_2-MnO-P_2O_5 diagram (Mullen, 1983). d) Th/Yb-Ta/Yb plot (Pearce, 1983). e) Ta-Yb diagram (Pearce *et al.*, 1984).

Fig. 13.- Diagramas de discriminación tectónica basados en elementos traza para las muestras de la Mélange de Somozas. a) Diagrama Ti-Zr-Y (Pearce and Cann, 1973). b) Diagrama Hf-Th-Ta (Wood, 1980). c) Diagrama TiO_2-MnO-P_2O_5 (Mullen, 1983). d) Diagrama Th/Yb-Ta/Yb (Pearce, 1983). Diagrama Ta-Yb (Pearce *et al.*, 1984).

mélange, are not observed to intrude island arc tholeiitic volcanic rocks. If these relationships are typical of the complete assemblage of igneous rocks in the ophiolitic mélange, these rocks may be remnants of a mature calc-alkaline volcanic arc that was affected by extension in a later stage and intruded by a new magmatic suite with the chemistry of island-arc tholeiites. The new U-Pb geochronology presented in this contribution includes the dating of two granitoids with calc-alkaline affinity (GCH-05-8 and GCH-05-6), and their ages strongly suggest that a mature volcanic arc was active during a great extent of the Cambrian (c. 500-527 Ma; Figs. 8 and 9). Geochronological data obtained from the conglomerate SO-3 suggest that the activity in this arc spanned the interval between the Ediacaran and the Early Ordovician. However, the youngest activity in the arc was probably residual because there are few detrital zircons with this age. Considering the age populations of the detrital zircons in this conglomerate, the activity in the volcanic arc represented in the Somozas Mélange probably occurred in a peri-Gondwanan setting, which is in agreement with the data obtained in similar rocks in the NW Iberian Massif and in the Bohemian Massif (Fernández Suárez *et al.*, 2002; Linnemann *et al.*, 2004).

The overall structure and evolution of the peri-Gondwanan arc preserved in the Somozas Mélange is similar to that presented in Figure 15, based on a model for the Lau Basin-Tonga Trench region (Hawkins, 2003). The model shows a mature calc-alkaline volcanic arc of Cambrian age, with the onset of the extensional activity in the arc resulting in the opening of intra-arc basins which were rapidly filled up with sediments as magmatism changed from calc-alkaline to island-arc tholeiites. According to previous data on the context and chronology for the opening of the Rheic Ocean (Murphy *et al.*, 2006; Arenas *et al.*, 2007a), it is acepted that continuous extension in the margin of Gondwana and the final rifting and the drift of Avalonia and related minor terranes, including fragments of the peri-Gondwanan arcs, finally caused the opening of this oceanic domain. In the NW of the Iberian Massif, the upper units of the allochthonous complexes contain igneous rocks with calc-alkaline and island-arc tholeiite affinities (Andonaegui *et al.*, 2002; Castiñeiras, 2005), with a chronology similar to that of the calc-alkaline rocks from the Somozas Mélange (c. 520-500 Ma). These units have been repeatedly interpreted as a fragment of a peri-Gondwanan arc rifted and finally drifted away from the main continent during the opening of the Rheic Ocean (Abati *et al.*, 1999, 2007; Gómez Barreiro *et al.*, 2007; Murphy and Gutiérrez Alonso, 2008). The new whole rock geochemistry and U-Pb geochronology data included in this contribution suggest an equivalence between both calc-alkaline series, which are interpreted to have been generated in the same Cambrian peri-Gondwanan volcanic-arc system.

6.2. Origin of the high-T tectonic blocks

A common characteristic to many ophiolitic mélanges is the presence of tectonic blocks with contrasting metamorphic conditions (Federico *et al.*, 2007; Kawai *et al.*, 2008). In this context, the presence in the Somozas Mélange of high-T tectonic blocks with orthogneisses and amphibolites may be explained by the incorporation in the mixing zone of rocks subducted to different depths that finally reached the low-viscosity serpentinite channel which forced their return. However, our data suggest that this straightforward interpretation may not apply in this case. The orthogneisses and amphibolites included in the high-T tectonic blocks show a tectonothermal evolution similar to some of the lithologies forming part of the Espasante Unit (Figs. 3 and 4), representing the basal units in the Cabo Ortegal Complex. Moreover, the U-Pb age obtained for the Gradoy orthogneiss (c. 485 Ma; Figs. 4 and 7) suggests affinity to the basal units of the allochthonous complexes, where the granitic magmatism is consistently younger (492-472 Ma) than in the upper units (520-500 Ma).

The basal units of the Cabo Ortegal Complex include the allochthonous terrane located on top of the Somozas Mélange, and they have been repeatedly interpreted as the most external margin of Gondwana subducted at the onset of the Variscan deformation. Even though the Somozas Mélange underlies the contact between the Moeche and Espasante units with out-of-sequence relationships (see the geological cross sections in Figs. 2 and 3), the basal units are those located in the lowest structural position in the terrane pile above the mélange zone and they are apparently involved in the generation of the mélange. The basal units were affected by high-P metamorphism at 370 Ma (Rodríguez *et al.*, 2003; Abati *et al.*, 2009), followed by a pronounced exhumation. The high-T tectonic blocks derived from the basal units are mixed in the mélange with lithologies affected by lower grade metamorphism, which suggests that they were incorporated in the mélange after the high-P event of c. 370 Ma, when the subducted margin of Gondwana experienced important rates of exhumation. The age of 370 Ma should be considered a maximum age limit for the generation of the Somozas Mélange.

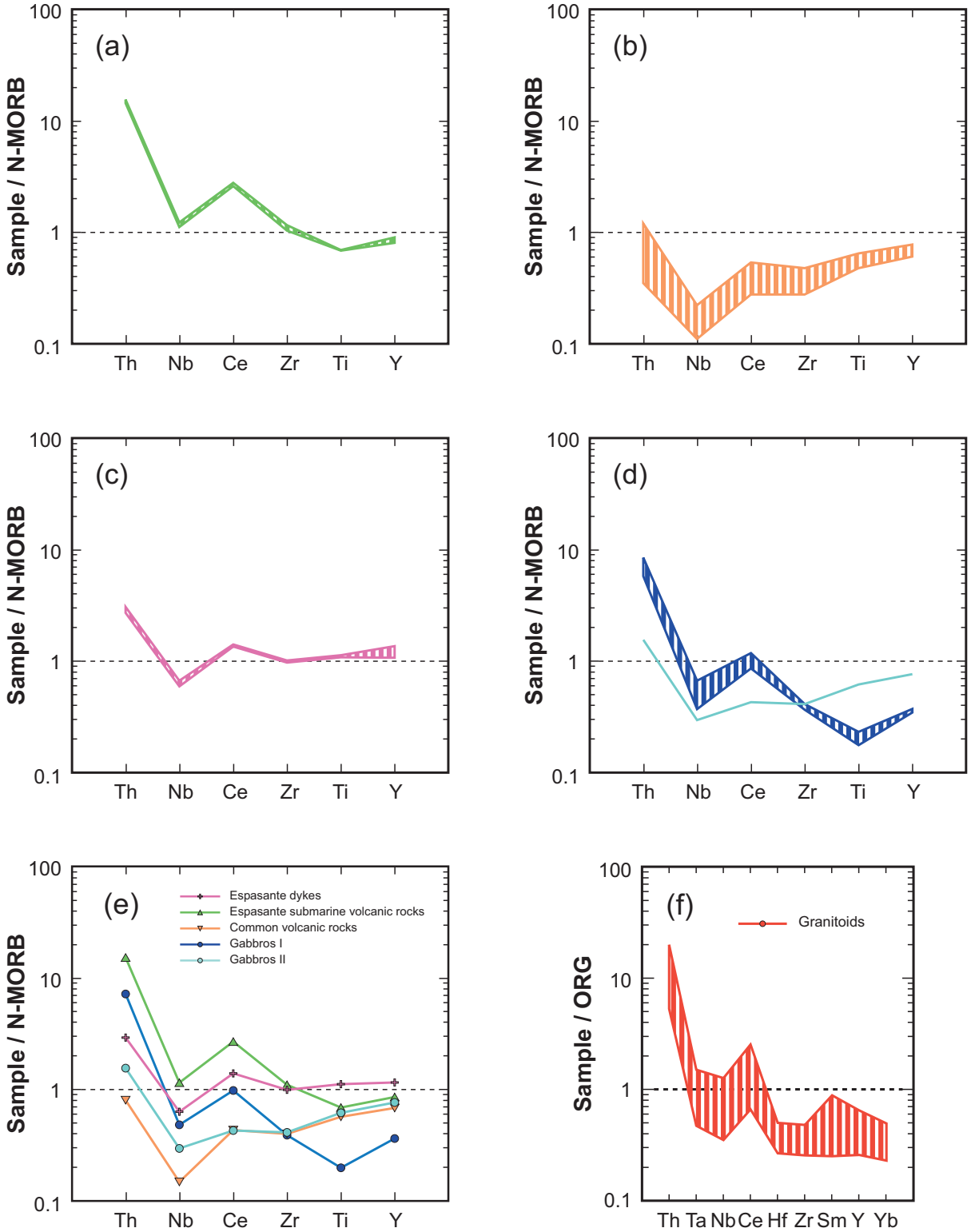

Fig. 14.- Immobile trace element plots of the most representative igneous rocks involved in the Somozas Mélange. Compositional ranges (a–d and f) and average compositions (e) are shown. Normalizing values in mafic rocks correspond to the N-MORB average composition according to Pearce (1996); normalizing values in granitoids are the ORG composition according to Pearce *et al.* (1984).

Fig. 14.- Proyecciones basadas en elementos traza inmóviles para los grupos ígneos más representativos que se encuentran en la Mélange de Somozas. Se indican los rangos de composición (a-e) y las composiciones medias (f). Los valores de normalización en las rocas básicas corresponden a la composición media del N-MORB propuesta por Pearce (1996); los valores de normalización en los granitoides corresponden a la composición media del ORG de acuerdo con Pearce *et al.* (1984).

6.3. Origin of the mélange unit and the assembly of Pangea

The identification of the high-T tectonic blocks as elements derived from the basal units of the allochthonous complexes, incorporated to the mélange after the c. 370 Ma subduction event and after important exhumation of the subducted margin, is important because it suggests that the Somozas Mélange represents a huge mixing unit directly located below the southern margin of Laurussia. The same conclusion can be inferred from the structural position of the mélange, which is located below the basal units of the allochthonous complexes and therefore in a more external position in the belt. Based on this evidence, it is not possible to relate the Somozas Mélange with the main subduction zone which affected the most external margin of Gondwana at the onset of the Variscan deformation. However, the relationship of the large ophiolitic mélanges with first order subduction zones have been clearly documented. It is therefore necessary to consider the existence of a secondary subduction zone developed behind the subducted margin of Gondwana,

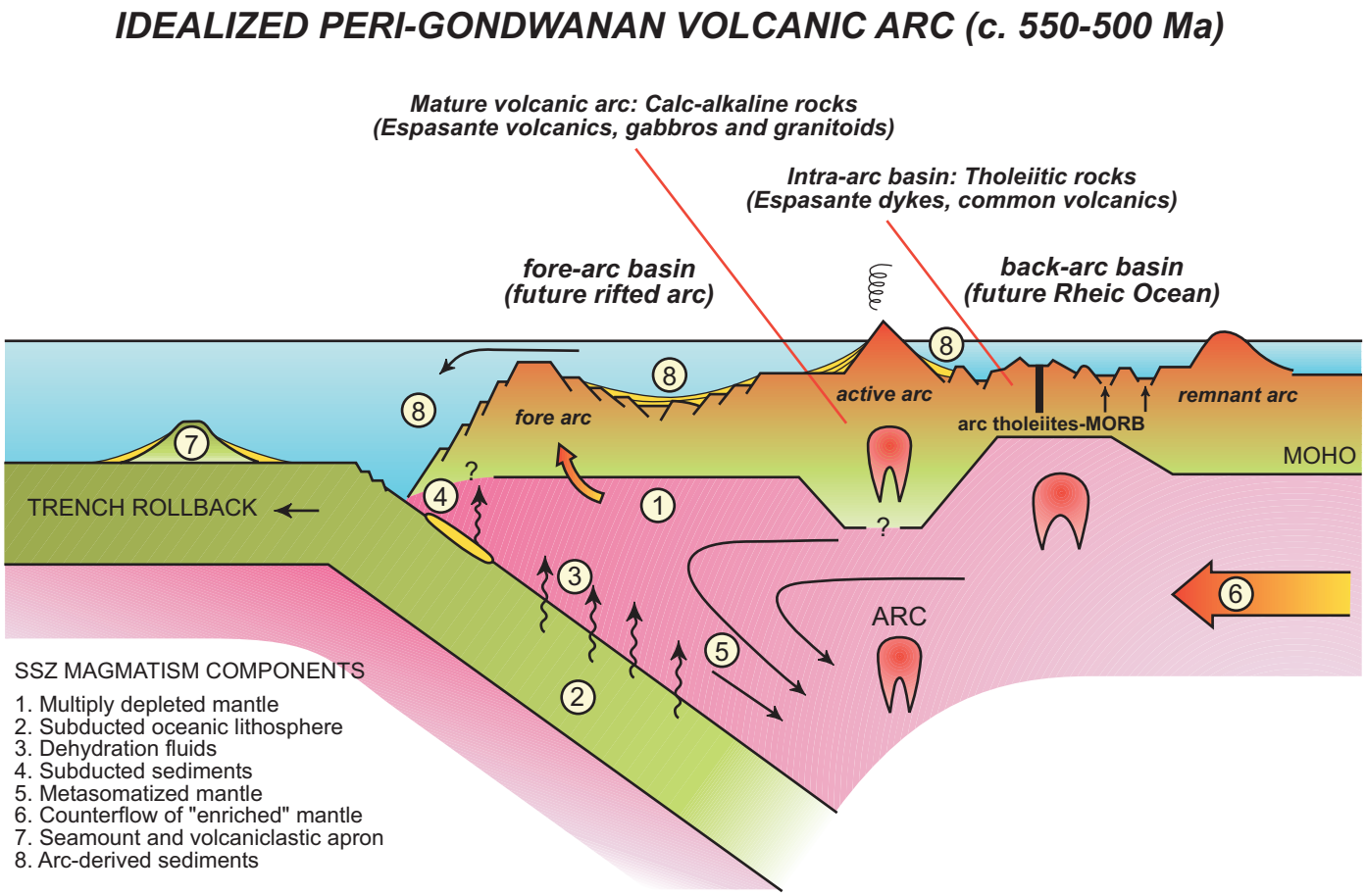

Fig. 15.- Cartoon showing an idealized peri-Gondwanan volcanic arc, its general structure and suggested future evolution based on the characteristics of the igneous lithologies involved in the Somozas Mélange and the geology of the allochthonous terranes in NW Iberia. The calc-alkaline rocks in the Somozas Mélange are correlated with remnants of a mature arc, which later on was affected by extension with generation of intra-arc basins with tholeiitic magmatism and abundant clastic sediments. The continuation of the extensional regime caused the rifting and drift of parts of the arc and their future accretion to the southern margin of Laurussia. Parts of this drifted arc are presently preserved in the upper allochthonous terrane in NW Iberia (upper units of the allochthonous complexes). The volcanic arc model is based on the Lau Basin – Tonga Trench region (Hawkins, 2003).

Fig. 15.- Esquema que representa un arco volcánico peri-Gondwánico idealizado, su estructura general y su posible evolución temporal, de acuerdo con las características de las rocas ígneas involucradas en la Mélange de Somozas y la geología de los terrenos alóctonos del NW de Iberia. Las rocas calco-alcalinas en la Mélange de Somozas representan los restos de un arco volcánico maduro, que posteriormente fue afectado por extensión con generación de cuencas intra-arco con magmatismo toleítico y abundantes sedimentos clásticos. La continuación del régimen extensional acabó generando la separación y deriva posterior de sectores de este arco, que terminaron por acrecionarse al margen meridional de Laurussia. Partes de este sistema de arcos están preservadas en la actualidad en el terreno alóctono superior del NW de Iberia (unidades superiores de los complejos alóctonos). El modelo de arco volcánico está basado en la Cuenca de Lau y en la Trinchera de Tonga (Hawkins, 2003).

closer to the continent. This subduction zone was apparently active only after the development of a pronounced decompression of the previously subducted continental margin (Fig. 16).

The geochemistry of igneous rocks and the U-Pb geochronology included in this contribution suggest that the ophiolitic mélange contains remnants of a Cambrian volcanic arc of peri-Gondwanan provenance. A similar volcanic arc does not exist in the most proximal sectors of the Gondwanan margin, presently located in the foreland zones of the belt. However, as has been discussed before, this volcanic arc shows identical characteristics to the arc-derived terrane located in the upper units of the allochthonous complexes, above the ophiolites generated during the closure of the Rheic Ocean, which define the main suture of the Variscan Belt (Fig. 16). The model purported to explain the origin of the Somozas Mélange should account fot the following facts: 1) the incorporation to the tectonic mélange of lithologies derived from the most external margin of Gondwana, previously subducted and affected by pronounced decompression; 2) the incorporation in the mélange of remnants of a Cambrian peri-Gondwanan arc, which in NW Iberia only has equivalence in the arc-derived terrane located in the upper units of the allochtonous complexes; 3) the generation of the mélange in a secondary subduction zone with

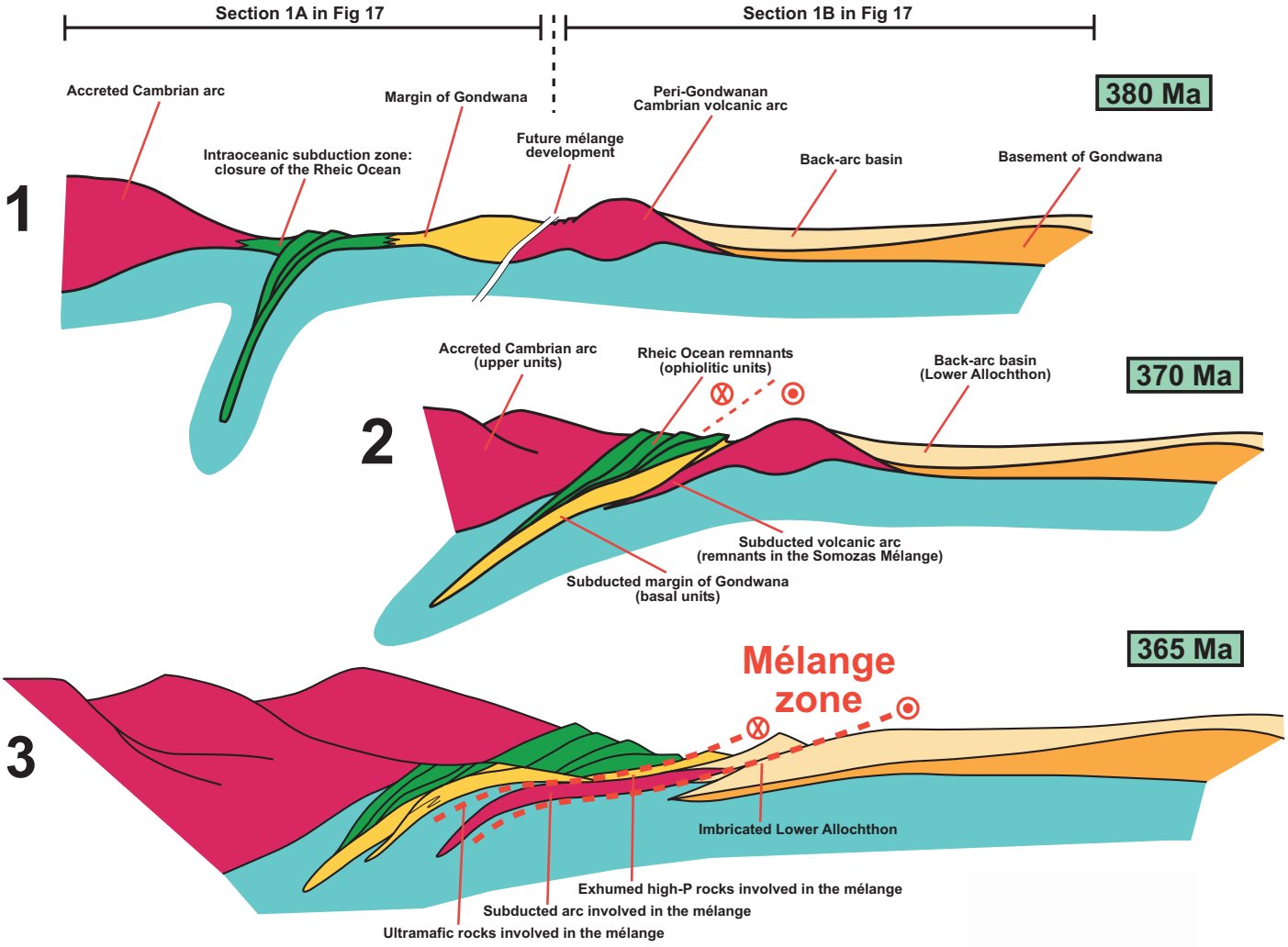

Fig. 16.- Schematic cross-sections showing some of the most significant geological events affecting the NW Iberia terranes during the Middle-Upper Devonian. They are related to the final assembly of Pangea and include: 1) closure of the Rheic Ocean by intraoceanic subduction at c. 380 Ma; 2) subduction directed to the north of the most external margin of Gondwana at c. 370 Ma; 3) final accretion of a remnant peri-Gondwanan arc and development of a large mélange zone.

Fig. 16.- Secciones esquemáticas que muestran algunos de los eventos geológicos más significativos que afectaron a los terrenos del NW de Iberia durante el Devónico Medio-Superior. Están relacionados con el ensamblado final de Pangea, e incluyen: 1) el cierre del Océano Rheico por subducción intraoceánica a los c. 380 Ma; 2) la subducción hacia el Norte del margen más externo de Gondwana a los c. 370 Ma; 3) la acreción final de un arco peri-Gondwánico residual y la generación de una gran zona de mélange.

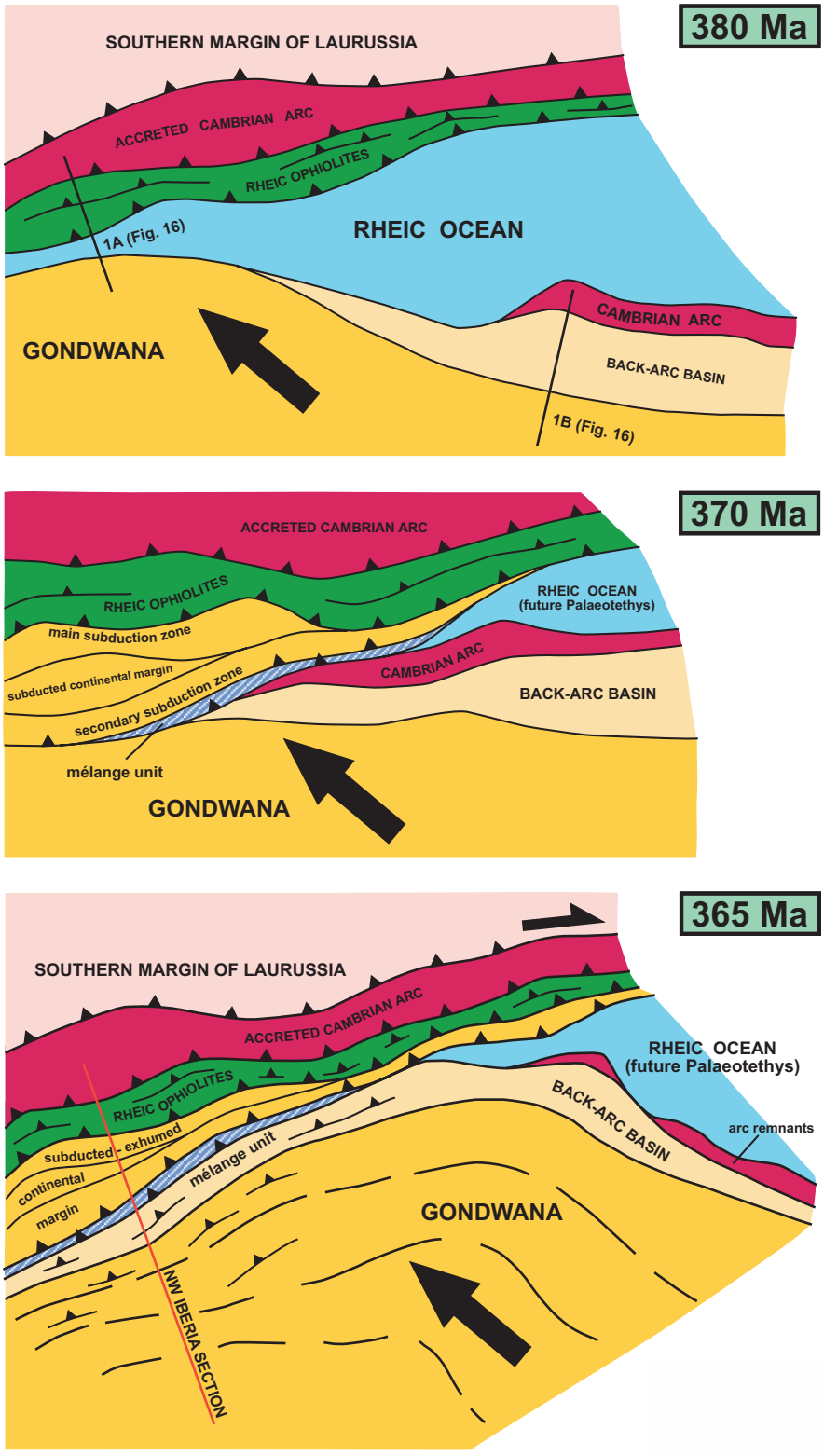

Fig. 17.- Terrane distribution and accretionary sequence during the last stages of the Pangea assembly. Oblique collision of Gondwana with an orogenic wedge previously developed in the southern margin of Laurussia caused subduction of the most external egde of the continent. Continuation of the oblique convergence favored the accretion of new remnants of the Cambrian peri-Gondwanan arc system. The development of a huge tectonic mélange in this context, the Somozas Mélange, suggests the generation of a secondary subduction zone. According to the tectonic blocks and slices which appear in the mélange, this mixing zone was developed in the contact area between exhumed high pressure rocks belonging to the marging of Gondwana and remnants of a Cambrian arc. Subsequent stages in the collision were characterized by the accretion of the Parautochthon or Lower Allochthon, with sedimentary sequences probably representing a back-arc basin, and the advance of deformation towards more internal regions of Gondwana.

Fig. 17.- Distribución de terrenos y secuencia acrecionaria durante los estadios finales del ensamblado de Pangea. La colisión oblicua de Gondwana con una cuña orogénica desarrollada previamente en el margen meridional de Laurussia, provocó la subducción del margen más externo del continente. La continuación de la colisión oblicua favoreció la acreción de nuevos restos del sistema de arcos cámbricos peri-Gondwánico. En este contexto, la generación de una gran mélange tectónica, la Mélange de Somozas, indica la existencia de una zona de subducción secundaria. De acuerdo con la naturaleza de los bloques y escamas tectónicos que aparecen en la mélange, esta zona de mezcla se desarrolló en la zona de contacto entre un conjunto de rocas de alta-P exhumadas y pertenecientes al margen de Gondwana, y los restos de una arco volcánico cámbrico. Los estadios posteriores de la colisión estuvieron caracterizados por la acreción del Parautóctono o Alóctono Inferior, que contiene secuencias sedimentarias probablemente representativas de una cuenca de trasera de arco, y por el avance de la deformación hacia regiones más internas de Gondwana.

activity after 370 Ma.

Figure 17 contains a comprehensive model explaining the most probable tectonic setting for the generation of the Somozas Mélange. It shows the distribution of allochthonous terranes in the southern margin of Laurussia, also to the south of Avalonia, which is firstly characterized by the accretion of a peri-Gondwanan terrane with volcanic-arc affinities and Cambrian age. U-Pb geochronological data, obtained in the upper units of the allochthonous complexes, for the high-P and high-T meta-

morphic event simultaneous to the accretion of this arc, suggest an age in the range 410-390 Ma (Ordóñez Casado *et al.*, 2001; Fernández-Suárez *et al.*, 2007). The accretion of this arc coincided with the beginning of the contraction in the Rheic Ocean. The final stages of the closure of this ocean were probably preceded by oblique convergence between Gondwana and Laurussia. Previously, an intra-Rheic subduction zone would have removed most of the old and cold lithosphere of the Rheic Ocean, generating in the Middle Devonian (c. 395 Ma) the supra-subduction zone ophiolites typical of the European Variscan Belt (Díaz García *et al.*, 1999; Sánchez Martínez *et al.*, 2007). The subduction of the most external margin of Gondwana should have started before 370 Ma, because this is the obtained age in the basal units of Galicia for the high-P metamorphism associated to this event (Rodríguez *et al.*, 2003; Abati *et al.*, 2009). This oblique subduction marks the beginning of the deformation in the most external margin of Gondwana, representing the first real Variscan deformation and metamorphism identified in the basement of western Europe. The progression of the oblique convergence and subduction was coeval with the exhumation of previously subducted continental sections, according to the process described by Platt (1986), and with the probable generation of a new secondary frontal subduction zone (Fig. 17). This new subduction zone represents the dynamic setting for the generation of the Somozas Mélange, and hence the place for the mixing of tectonic blocks derived from the basal units (high-T tectonic blocks) and the remnants of a Cambrian peri-Gondwanan volcanic-arc similar to that exposed in the upper units of the allochthonous complexes. The continuation of the convergence derived in a transition towards an intracontinental setting and the blocking of the activity in the secondary subduction zone. The deformation advanced towards the most external zones of the belt, favoring the accretion of the Parautochthon to the orogenic wedge, probably representing a restricted basin located between the volcanic-arc system and the continent, and finally the accretion of the autochthonous domain.

The suggested model is compatible with the terrane distribution in the NW of the Iberian Massif and also with the overall structure of the orogenic wedge in this sector of the belt. It also allows to explain one of the most enigmatic aspects in the Somozas Mélange, such as the incorporation to the mixing unit of the remnants of a terrane with volcanic-arc affinity. In the NW Iberian Massif, this terrane does not exist below the suture zone defined by the ophiolitic units. The model also explains the existence in the mélange of high-T tectonic blocks. Finally, it also presents a dynamic context for the generation of the tectonic mélange related to the activity of an important subduction zone, a characteristic in most ophiolitic mélanges. The Somozas Mélange is connected to one of the most important contacts developed in the basement of western Europe during the assembly of Pangea. Its continuation could be expected across the French Massif Central and the Bohemian Massif, where the allochthonous complexes described in NW Iberia can be recognized (Martínez Catalán *et al.*, 2007). The identification of equivalent units in these regions will enable further correlation of the allochthonous terranes involved in the Pangea suture. However, a similar mélange has not yet been described in the rest of the Variscan Belt.

Acknowledgements

Financial support for this research has been provided by Spanish project CGL2007-65338-CO2-01/BTE (Ministerio de Ciencia e Innovación). The authors thank José Ramón Martínez Catalán and Javier Fernández Suárez for field cooperation and mineral separation, respectively. Juan Gómez Barreiro and Wayne Premo are kindly acknowledged for their assistance during the SHRIMP analytical sessions as well as the staff from the Denver Microbeam Laboratoire (USGS) and the SUMAC facility. SSM especially acknowledges the analytical facilities provided by the Natural History Museum of London through financial support of the European Union Synthesys Project. This study is also a contribution to the IGCP 497, "The Rheic Ocean: Origin, evolution and correlatives". Brendan Murphy and Jean Paul Liégeois are kindly acknowledged for insightful reviews of the manuscript.

References

Abati, J., Dunning, G.R., Arenas, R., Díaz García, F., González Cuadra, P., Martínez Catalán, J.R., Andonaegui, P. (1999): Early Ordovician orogenic event in Galicia (NW Spain): evidences from U-Pb ages in the uppermost unit of the Órdenes Complex. *Earth and Planetary Science Letters*, 165: 213-228.

Abati, J., Castiñeiras, P., Arenas, R., Fernández-Suárez, J., Gómez-Barreiro, J., Wooden, J. (2007): Using SHRIMP zircon dating to unravel tectonothermal events in arc environments. The early Palaeozoic arc of NW Iberia revisited. *Terra Nova*, 19: 432-439.

Abati, J., Gerdes, A., Fernández-Suárez, J., Arenas, R., Whitehouse, M.J., Díez Fernández, R. (2009): Magmatism and early-Variscan continental subduction in the northern Gondwana margin recorded in zircons from the basal units of Galicia, NW Spain. *Geological Society of America Bulletin.* In press.

Andonaegui, P., González del Tánago, J., Arenas, R., Abati, J., Martínez Catalán, J.R., Peinado, M., Díaz García, F. (2002):

Tectonic setting of the Monte Castelo gabbro (Órdenes Complex, northwestern Iberian Massif): Evidence for an arc-related terrane in the hanging wall to the Variscan suture. In: J.R. Martínez Catalán, R.D. Hatcher Jr., R. Arenas, F. Díaz García (eds.), *Variscan-Appalachian Dynamics: the building of the Late Paleozoic Basement*. Geological Society of America Special Paper, 364: 37-56.

Arenas, R. (1985): Evolución petrológica y geoquímica de la unidad alóctona inferior del complejo metamórfico básico-ultrabásico de Cabo Ortegal (Unidad de Moeche) y del Silúrico paraautóctono, Cadena Hercínica Ibérica (NW de España). *Tesis Doctoral. Universidad Complutense de Madrid*: 543 p.

Arenas, R., Peinado, M. (1981): Presencia de pillow-lavas en las metavolcanitas submarinas de las proximidades de Espasante, Cabo Ortegal, NW de España. *Cuadernos de Geología Ibérica*, 7: 105-119.

Arenas, R., Gil Ibarguchi, J.I., González Lodeiro, F., Klein, E., Martínez Catalán, J.R., Ortega Gironés, E., Pablo Macía, J.G. de, Peinado, M. (1986): Tectonoestratigraphic units in the complexes with mafic and related rocks of the NW of the Iberian Massif. *Hercynica*, II: 87-110.

Arenas, R., Rubio Pascual, F.J., Díaz García, F., Martínez Catalán, J.R. (1995): High-pressure microinclusions and development of an inverted metamorphic gradient in the Santiago Schists (Órdenes Complex, NW Iberian Massif, Spain): evidence of subduction and syn-collisional decompression. *Journal of Metamorphic Geology*, 13: 141-164.

Arenas, R., Abati, J., Martínez Catalán, J.R., Díaz García, F., Rubio Pascual, F.J. (1997): P-T evolution of eclogites from the Agualada Unit (Órdenes Complex, NW Iberian Massif, Spain): Implications for crustal subduction. *Lithos*, 40: 221-242.

Arenas, R., Martínez Catalán, J.R., Sánchez Martínez, S., Fernández-Suárez, J., Andonaegui, P., Pearce, J.A., Corfu, F. (2007a): The Vila de Cruces Ophiolite: A remnant of the Early Rheic Ocean in the Variscan suture of Galicia (Northwest Iberian Massif). *Journal of geology*, 115: 129-148.

Arenas, R., Sánchez Martínez, S., Castiñeiras, P., Fernández Suárez, J., Jeffries, T. (2007b): Geochemistry and geochronology of the ophiolite involved in the Somozas mélange: new insights on the birth of the Rheic Ocean. In: R. Arenas, J.R. Martínez Catalán, J. Abati, S. Sánchez Martínez (eds.), *The rootless Variscan suture of NW Iberia (Galicia, Spain). The International Geoscience Programme, IGCP 497. Galicia Meeting 2007. Field trip guide & Conference abstracts.* Publicaciones del Instituto Geológico y Minero de España: 151-153.

Arenas, R., Sánchez Martínez, S., Castiñeiras, P., Fernández-Suárez, J., Díez Fernández, R., Jeffries, T.E. (2008): The basal tectonic mélange of the Cabo Ortegal Complex (NW Spain): Rock assemblages, involved terranes and paleogeographic scenario for the suture of Pangea. In: P. Königshof, U. Linneman (eds.), *From Gondwana and Laurussia to Pangaea: Dynamics of oceans and supercontinents. The International Geoscience Programme, IGCP 497 and IGCP 499. 20th International Senckenberg-Conference & 2nd Geinitz-Conference*. Abstracts and Programme: 19-21.

Black, L.P., Kamo, S.L., Allen, C.M., Davis, D.W., Aleinikoff, J.N., Valley, J.W., Mundil, R., Campbell, I.H., Korsch, R.J., Williams, I.S., Foudoulis, C. (2004): Improved $^{206}Pb/^{238}U$ microprobe geochronology by the monitoring of a trace-element-related matrix effect, SHRIMP, ID-TIMS, ELA-ICP-MS and oxygen isotope documentation for a series of zircon standards. *Chemical Geology*, 205: 115-140.

Castiñeiras, P. (2005): Origen y evolución tectonotermal de las unidades de O Pino y Cariño (Complejos Alóctonos de Galicia). *Nova Terra*, 28: 279 p.

Corfu, F., Hanchar, J.M., Hoskin, P.W.O., Kinny, P. (2003): Atlas of zircon textures. In: J.M. Hanchar, P.W.O. Hoskin (eds.). *Zircon*. Mineralogical Society of America, Washington. Reviews in Mineralogy and Geochemistry, 53: 468-500.

Dallmeyer, R.D., Martínez Catalán, J.R., Arenas, R., Gil Ibarguchi, J.I., Gutiérrez Alonso, G., Farias, P., Aller, J., Bastida, F. (1997): Diachronous Variscan tectonothermal activity in the NW Iberian Massif: evidence from $^{40}Ar/^{39}Ar$ dating of regional fabrics. *Tectonophysics*, 277: 307-337.

Díaz García, F., Arenas, R., Martínez Catalán, J.R., González del Tánago, J., Dunning, G.R. (1999): Tectonic evolution of the Careón Ophiolite (northwest Spain): a remnant of oceanic lithosphere in the Variscan Belt. *Journal of Geology*, 107: 587-605.

Federico, L., Crispini, L., Scambelluri, M., Capponi, G. (2007): Ophiolite mélange zone records exhumation in a fossil subduction channel. *Geology*, 35: 499-502.

Fernández-Suarez, J., Corfu, F., Arenas, R., Marcos, A., Martínez Catalán, J.R., Díaz García, F., Abati, J., Fernández, F.J. (2002): U-Pb evidence for a polymetamorphic evolution of the HP-HT units of the NW Iberia Massif. *Contributions to Mineralogy and Petrology*, 143: 236-253.

Fernández-Suárez, J., Díaz García, F., Jeffries, T.E., Arenas, R., Abati, J. (2003): Constraints on the provenance of the uppermost allochthonous terrane of the NW Iberian Massif: Inferences from detrital zircon U-Pb ages. *Terra Nova*, 15: 138-144.

Fernández Suárez, J., Arenas, R., Abati, J., Martínez Catalán, J.R., Whitehouse, M.J., Jeffries, T.E. (2007): U-Pb chronometry of polymetamorphic high-pressure granulites: An example from the allochthonous terranes of the NW Iberian Variscan belt. In: R.D. Hatcher Jr., M.P. Carlson, J.H. McBride, J.R. Martínez Catalán (eds.), *4-D Framework of Continental Crust*. Geological Society of America Memoir, 200: 469-488.

Gerya, T.V., Stockhert, B., Perchuk, A.L. (2002): Exhumation of high-pressure metamorphic rocks in a subduction channel: a numerical simulation. *Tectonics*, 21 (6), Art No. 1056.

Gómez Barreiro, J., Martínez Catalán, J.R., Arenas, R., Castiñeiras, P., Abati, J., Díaz García, F., Wijbrans, J.R. (2007): Tectonic evolution of the upper allochthon of the Órdenes complex (northwestern Iberian Massif): Structural constraints to a polyorogenic peri-Gondwanan terrane. In: U. Linneman, R.D. Nance, P. Kraft, G. Zulauf (eds.), *The evolution of the Rheic Ocean: From Avalonian-Cadomian active margin to Alleghenian-Variscan collision.* Geological Society of America Special Paper, 423: 315-332.

Guilmette, C., Hébert, R., Dupuis, C., Wang, C, Li, Z. (2008): Metamorphic history and geodynamic significance of high-grade metabasites from the ophiolitic mélange beneath the Yarlung Zangbo ophiolites, Xigaze area, Tibet. *Journal of Asian Earth Sciences*, 32: 423-437.

Hawkins, J.W. (2003): Geology of supra-subduction zones - Implications for the origin of ophiolites. In: Y. Dilek, S. Newcomb (eds.), *Ophiolite concept and the evolution of geological thought*. Geological Society of America Special Paper, 373: 227-268.

Hefferan, K.P., Admou, H., Hilal, R., Karson, J.A., Saquaque, A., Juteau, T., Bohn, M.M., Samson, S.D., Kornprobst, J.M. (2002): Proterozoic blueschist-bearing mélange in the Anti-Atlas Mountains, Morocco. *Precambrian Research*, 118: 179-194.

Hirauchi, K., Tamura, A., Arai, S., Yamaguchi, H., Hisada, K. (2008): Fertile abyssal peridotites within the Franciscan subduction complex, central California: Possible origin as detached remnants of oceanic fracture zones located close to a slow-spreading ridge. *Lithos*, 105: 319-328.

Ireland, T.R., Williams, I.S. (2003): Considerations in zircon geochronology by SIMS. In: J.M Hanchar, P.W.O. Hoskin (eds). *Zircon*. Mineralogical Society of America, Washington. Reviews in Mineralogy and Geochemistry, 53: 215-241.

Jeffries, T., Fernández-Suárez, J., Corfu, F., Gutiérrez-Alonso, G. (2003): Advances in U–Pb geochronology using a frequency quintupled Nd:YAG based laser ablation system (lambda = 213nm) and quadrupole based ICPMS. *Journal of Analytical Atomic Spectrometry*, 18: 847–855.

Kato, K., Saka, Y. (2003): Kurosegawa terrane as a transform fault zone in southwest Japan. *Gondwana Research*, 6: 669-686.

Kawai, T., Windley, B.F., Shibuya, T., Omori, S., Sawaki, Y., Maruyama, S. (2008): Large P-T gap between Ballantrae blueschist/garnet pyroxenite and surrounding ophiolite, southern Scotland, UK: Diapiric exhumation of a Caledonian serpentinite mélange. *Lithos*, 104: 337-354.

Le Maitre, R.W., Bateman, P., Dudek, A., Keller, J., Lameyre Le Bas, M.J., Sabine, P.A., Schmid, R., Sorensen, H., Streckeisen, A., Wooley, A.R., Zanettin, B. (1989): *A classification of igneous rocks and glossary of terms.* Blackwell Scientific Publications, Oxford: 193 p.

Linnemann, U., McNaughton, N.J., Romer, R.L., Gehmlich, M., Drost, K., Tonk., C. (2004): West African provenance for Saxo-Thuringia (Bohemian Massif): Did Armorica ever leave pre-Pangean Gondwana? – U/Pb-SHRIMP zircon evidence and the Nd-isotopic record. *International Journal of Earth Sciences*, 93: 683-705.

Ludwig, K.R. (2002): *SQUID 1.02, a user's manual*. Berkeley Geochronology Center Special Publication, 2: 17 p.

Ludwig, K.R. (2003): *ISOPLOT/Ex, version 3, A Geochronological Toolkit for Microsoft Excel*. Berkeley Geochronology Center Special Publication, 4: 71 p.

MacPherson, G.J., Giaramita, M.J., Phipps, S.P. (2006): Tectonic implications of diverse igneous blocks in Franciscan mélange, Northern California and southwestern Oregon. *American Mineralogist*, 91: 1509-1520.

Mahéo, G., Fayoux, X., Guillot, S., Garzanti, E., Capiez, P., Mascle, G. (2006): Relicts of an inra-oceanic arc in the Sapi-Shergol mélange zone (Ladakh, NW Himalaya, India): implications for the closure of the Neo-Tethys Ocean. *Journal of Asian Earth Sciences*, 26: 695-707.

Marcos, A., Farias, P., Galán, G., Fernández, F.J., Llana-Fúnez, S. (2002): Tectonic framework of the Cabo Ortegal Complex: A slab of lower crust exhumed in the Variscan orogen (northwestern Iberian Peninsula). In: J.R. Martínez Catalán, R.D. Hatcher Jr., R. Arenas, F. Díaz García (eds.), *Variscan-Appalachian Dynamics: the building of the Late Paleozoic Basement*. Geological Society of America Special Paper, 364: 143-162.

Martínez Catalán, J.R., Arenas, R., Díaz García, F., Rubio Pascual, F.J., Abati, J., Marquínez, J. (1996): Variscan exhumation of a subducted Paleozoic continental margin: The basal units of the Órdenes Complex, Galicia, NW Spain. *Tectonics*, 15: 106-121.

Martínez Catalán, J.R., Díaz García, F., Arenas, R., Abati, J., Castiñeiras, P., González Cuadra, P., Gómez Barreiro, J., Rubio Pascual, F. (2002): Thrust and detachment systems in the Órdenes Complex (northwestern Spain): Implications for the Variscan-Appalachian geodynamics. In: J.R. Martínez Catalán, R.D. Hatcher Jr., R. Arenas, F. Díaz García (eds.), *Variscan-Appalachian Dynamics: the building of the Late Paleozoic Basement*. Geological Society of America Special Paper, 364: 163-182.

Martínez Catalán, J.R., Arenas, R., Díaz García, F., González Cuadra, P., Gómez-Barreiro, J., Abati, J., Castiñeiras, P., Fernández-Suárez, J., Sánchez Martínez, S., Andonaegui, P., González Clavijo, E., Díez Montes, A., Rubio Pascual F.J., Valle Aguado, B. (2007): Space and time in the tectonic evolution of the northwestern Iberian Massif: Implications for the Variscan belt. In: R.D. Hatcher Jr., M.P. Carlson, J.H. McBride, J.R. Martínez Catalán (eds.), *4-D Framework of Continental Crust.* Geological Society of America Memoir, 200: 403-423.

Martínez Catalán, J.R., Fernández-Suárez, J., Meireles, C., Clavijo, E.G., Belousova, E., Saeed, A. (2008): U-Pb detrital zircon ages in synorogenic deposits of the NW Iberian Massif (Variscan belt). Interplay of Devonian-Carboniferous sedimentation and thrust tectonics. *Journal of The Geological Society*, 165: 687-698.

Matte, Ph. (1991): Accretionary history and crustal evolution of the Variscan belt in Western Europe. *Tectonophysics*, 196: 309-337.

Mullen, E.D. (1983): MnO/TiO2/P2O5: a minor element discriminant for basaltic rocks of oceanic environments and its aplications for petrogenesis. *Earth and Planetary Science Letters*, 62: 53-62.

Murphy, J.B., Gutiérrez-Alonso, G., Nance, R.D., Fernández-Suárez, J., Keppie, J.D., Quesada, C., Strachan, R.A., Dostal, J. (2006): Origin of the Rheic Ocean: rifting along a Neoproterozoic suture? *Geology*, 34: 325-328.

Murphy, J.B., Gutiérrez-Alonso, G. (2008): The origin of the Variscan upper allochthons in the Ortegal Complex, northwestern Iberia: Sm-Nd isotopic constraints on the closure of

the Rheic Ocean. *Canadian Journal of Earth Science*, 45: 651-668.

Nakamura, N. (1974): Determination of REE, Ba, Fe, Mg, Na and K in carbonaceous and ordinary condrites. *Geochemica et Cosmochimica Acta*, 38: 757-775.

Nance, R.D., Murphy, J.B. (1994): Contrasting basement signatures and the palinspastic restoration of peripheral orogens: example from Neoproterozoic Avalonian-Cadomian belt. *Geology*, 22: 617-620.

Norman, M.D., Pearson, N.J., Sharma, A.A., Griffin, W.L. (1996): Quantitative analysis of trace elements in geological materials by laser ablation ICPMS: instrumental operating conditions and calibration values of NIST glasses. *Geostandards Newsletter*, 20: 247-261.

Oczlon, M.S. (2006): Terrane map of Europe. *Gaea Heidelbergensis*, 15.

Ordoñez Casado, B., Gebauer, D., Schäfer, H.J., Gil Ibarguchi, J.I., Peucat, J.J. (2001): A single Devonian subduction event for the HP/HT metamorphism of the Cabo Ortegal complex within the Iberian Massif. *Tectonophysics*, 332: 359-385.

Osmaston, M.F. (2008): Basal subduction tectonic erosion (STE), butter mélanges, and the construction and exhumation of HP-UHP belts: The Alps example and some comparisons. *International Geology Review*, 50: 685-754.

Pearce, J.A. (1983): Role of the sub-continental lithosphere in magma genesis at active continental margins. In: C.J. Hawkesworth, M.J. Norry (eds.), *Continental basalts and mantle xenoliths*. Shiva, Nantwich: 230-249.

Pearce, J.A. (1996): A users guide to basalt discrimination diagrams. In: D.A. Wyman (ed.), *Trace Element Geochemistry of Volcanic Rocks: Applications for Massive Sulphide Exploration*. Short Course Notes. Geological Association of Canada, 12: 79-113.

Pearce, J.A., Cann, J.R. (1973): Tectonic setting of basic volcanic rocks determined using trace element analyses. *Earth and Planetary Science Letters*, 19: 290-300.

Pearce, J.A., Harris, N.B.W., Tindle, A.G. (1984): Trace element discrimination diagrams for the tectonic interpretation of granitic rocks. *Journal of Petrology*, 25: 956-983.

Pearce, J.A., Parkinson, I.J. (1993): Trace element models for mantle melting; application to volcanic arc petrogenesis. In: H.M. Prichard, T. Alabaster, N.B.W. Harris, C.R. Neary (eds.), *Magmatic processes and plate tectonics*. Geological Society Special Publications, 76: 373-403.

Pidgeon, R.T., Furfaro, D., Kennedy, A.K., Nemchin, A.A., van Bronswjk, W. (1995): *Calibration of zircon standards for the Curtin SHRIMP II*. U.S. Geological Survey Circular, 1107: 251.

Platt, J.P. (1986): Dynamics of orogenic wedges and the uplift of high-pressure metamorphic rocks. *Geological Society of America Bulletin*, 97: 1037-1053.

Rodríguez, J., Cosca, M.A., Gil Ibarguchi, J.I., Dallmeyer, R.D. (2003): Strain partitioning and preservation of $^{40}Ar/^{39}Ar$ ages during Variscan exhumation of a subducted crust (Malpica-Tui complex, NW Spain). *Lithos*, 70: 111-139.

Sánchez Martínez, S., Arenas, R., Díaz García, S., Martínez Catalán, J.R., Gómez Barreiro, J., Pearce, J. (2007): The Careón Ophiolite, NW Spain: supra-subduction zone setting for the youngest Rheic Ocean floor. *Geology*, 35: 53-56.

Stacey, J.S., Kramers, J.D. (1975): Approximation of terrestrial lead isotope evolution by a two-stage model. *Earth Planetary Science Letters*, 26: 207-221.

Stöckhert, B., Gerya, T.V. (2005): Pre-collisional high pressure metamorphism and nappe tectonics at active continental margins: a numerical simulation. *Terra Nova*, 17: 102-110.

Taylor, S.R., McLennan, S.M. (1985): *The continental crust: its composition and evolution*. Blackwell, Oxford: 328 p.

Valverde-Vaquero, P., Marcos, A., Farias, P., Gallastegui, G. (2005): U-Pb dating of Ordovician felsic volcanism in the Schistose Domain of the Galicia-Trás-os-Montes Zone near Cabo Ortegal (NW Spain). *Geologica Acta*, 3: 27-37.

Van der Meer Mohr, C.G. (1975): The Palaeozoic strata near Moeche in Galicia, NW Spain. *Leidse Geologische Mededelingen*, 49: 33-37.

Williams, I.S. (1997): U-Th-Pb geochronology by ion microprobe: not just ages but histories. *Economic Geology*, 7: 1-35.

Winchester, J.A., Floyd, P.A. (1977): Geochemical discrimination of different magma series and their differentiation products using inmobile elements. *Chemical Geology*, 20: 325-343.

Wood, D.A. (1980): The application of a Th-Hf-Ta diagram to problems of tectonomagmatic classification and to establishing the nature of crustal contamination of basaltic lavas of the British Tertiary Volcanic Province. *Earth and Planetary Science Letters*, 50: 11-30.

Zhang, Q., Wang, C.Y., Liu, D., Jian, P., Qian, Q., Zhou, G., Robinson, P.T. (2008): A brief review of ophiolites in China. *Journal of Asian Earth Sciences*, 32: 308-324.